Palaeontologia Electronica
palaeo-electronica.org

Late Jurassic ichthyosaurs from southern Germany

Erin E. Maxwell, Jule Neumann, and Giovanni Serafini

ABSTRACT

The Tithonian (Late Jurassic) represents a high point in ichthyosaurian taxonomic diversity, although ecomorphological disparity is not correspondingly high. Numerous fossil lagerstätte from a range of palaeolatitudes in both the Northern and Southern Hemispheres are thought to be responsible for the high observed generic diversity during this time interval; however, faunal provincialism has also been proposed as a driver. Here, we re-evaluate the ichthyosaur fauna of the German Plattenkalk deposits and provide a revised estimate for taxonomic diversity from these fossil lagerstätten. Unlike coeval lagerstätten, only a single accepted ichthyosaurian genus from the Late Jurassic of Germany, *Aegirosaurus leptospondylus,* has been described to date, suggesting considerable undersampling. Here, we describe a second genus from these deposits, *Jabalisaurus tethyensis* sp. nov., based on material previously included within *Aegirosaurus*. New observations provide additional details on the osteology, soft tissue morphology, and diet in *J. tethyensis. Jabalisaurus* was previously known only from the Late Jurassic of Mexico. The presence of this genus in Europe leads us to reject the faunal provincialism hypothesis, and suggests instead the existence of a unique Peri-Tethyan ichthyosaurian fauna, distinct from both the Boreal/sub-Boreal and Eastern Pacific faunas and potentially controlled by climatic variables.

Erin E. Maxwell. Staatliches Museum für Naturkunde Stuttgart, Rosenstein 1, 70191 Stuttgart, Germany; erin.maxwell@smns-bw.de
Jule Neumann. Fichtner GmbH & Co. KG, Stuttgart, Germany; jule.neumann@neumann-besigheim.de
Giovanni Serafini. Dipartimento di Scienze Chimiche e Geologiche, Università di Modena e Reggio Emilia, Via Campi 103, 41125 Modena, Italy; giovanni.serafini@unimore.it

Keywords: Ichthyosauria; Ophthalmosauria; Plattenkalk; Altmühltal Formation; Torleite Formation; new species

Submission: 18 February 2026. Acceptance: 9 July 2026.

https://zoobank.org/E557598D-F3C2-4AD2-A578-92E1A9BE98C3

Final citation: Maxwell, Erin E., Neumann, Jule, and Serafini, Giovanni. 2026. Late Jurassic ichthyosaurs from southern Germany. Palaeontologia Electronica, 29(2):a30.
https://doi.org/10.26879/1676
palaeo-electronica.org/content/2026/5919-late-jurassic-ichthyosaurs-from-germany

INTRODUCTION

Ichthyosaurs are Mesozoic marine reptiles that first appeared in the fossil record in the Early Triassic and persisted until the early Late Cretaceous (McGowan and Motani, 2003). The high point of ichthyopterygian diversity and disparity is widely understood to have been attained during the first ~8.7 million years of the group's evolution (Flannery Sutherland et al., 2019), attributed to high rates of morphological evolution early in the history of the clade during their initial radiation into diverse marine habitats and dietary niches (Moon and Stubbs, 2020). By the Jurassic, and especially by the end of the Aalenian (early Middle Jurassic), ichthyosaurs occupied a reduced range of ecomorphotypes (Fischer et al., 2021), and historically were viewed as being correspondingly reduced in taxonomic diversity (Sander, 2000).

In contrast to the historical view, over the past 20 years it has become evident that the Tithonian (Late Jurassic) represents a high point in raw ichthyosaurian taxonomic diversity, despite relatively low ecomorphological disparity (Fischer et al., 2014; Cleary et al., 2015; Fernández and Campos, 2015; Flannery Sutherland et al., 2019; Barrientos-Lara and Alvarado-Ortega, 2021a). The dynamics driving this pattern have yet to be been resolved: lagerstätte effects are considered to be the most likely underlying cause (Benson et al., 2010), with the Tithonian record far surpassing any other Jurassic stage in global representation of lagerstätte-quality open marine deposits, although faunal provincialism has also been proposed as a driver (Barrientos-Lara and Alvarado-Ortega, 2021a).

Ichthyosaur-bearing localities spanning high to mid-latitudes in the northern hemisphere are well-represented in the Kimmeridgian-Tithonian record and tend to show extensive taxon overlap at the generic level (Svalbard, the UK, and Volga regions: Zverkov and Efimov, 2019; Zverkov and Prilepskaya, 2019; Zverkov and Jacobs, 2020). In contrast, localities in Mexico and Argentina show a high degree of endemism (Barrientos-Lara and Alvarado-Ortega, 2021a), with few to no genera shared either with each other or with the European localities. The ichthyosaur assemblage of southern Germany is very poorly documented, but the invertebrate fauna has a more Tethyan character than that of other European localities (sub-Mediterranean Province vs. Boreal or sub-Boreal Provinces: Cecca, 1999; Westermann, 2000), and thus might provide new insights into the degree of faunal overlap or relatedness in ichthyosaurs between Europe and Mexico.

Ichthyosaurian fossils from the Late Jurassic Bavarian Plattenkalk deposits of Germany were first described during the 1850s, comprising what is now understood to be a multi-taxic assemblage (reviewed by Bardet and Fernández, 2000). None of this original material has survived into the present day, and due to the loss of this historical material, only a single monotypic genus is documented from the German Late Jurassic: *Aegirosaurus* Bardet and Fernández, 2000. At the time of genus naming, only six ophthalmosaurian genera were accepted as valid: *Ophthalmosaurus, Brachypterygius, Caypullisaurus, Mollesaurus, Platypterygius,* and *Nannopterygius*. Since that time, however, the number of ophthalmosaurian genera has undergone a dramatic increase, with at least 21 genera recognized depending on the author. The description of *Aegirosaurus leptospondylus*, while sufficient 25 years ago, is no longer detailed enough to accurately score characters in phylogenetic matrices. Moreover, it has become clear that specimens referred to this species are not congeneric with the neotype. Here, we remove SNSB-BSPG 1954 I 608 from the concept of *Aegirosaurus*, provide a revised diagnosis for the genus, and assign most of the referred material to a new species in the genus *Jabalisaurus*, to date described only from Mexico.

Institutional abbreviations. SM, Schwegler Museum, Langenaltheim, Germany; **SNSB-BSPG**, Bayerische Staatssammlung für Paläontologie und Geologie, Munich, Germany; **JME**, Jura-Museum Eichstätt, Eichstätt, Germany; **MUDE**, Museo del Desierto, Saltillo, Coahuila, Mexico; **NHMUK**, Natural History Museum, London, UK; **SMNS**, Staatliches Museum für Naturkunde Stuttgart, Germany.

Previous Work on Ichthyosaurs from the Bavarian Plattenkalks and the Genus *Aegirosaurus*

The first ichthyosaurian taxon to be named from the Late Jurassic of Bavaria was *Ichthyosaurus posthumus* Wagner, 1852 from the Late Jurassic of Kelheim. This species was based on an isolated tooth and is now considered to be a nomen dubium (McGowan, 1976). *Ichthyosaurus leptospondylus* was named the following year based on the so-called Oberndorfer specimen, also from Kelheim (Wagner, 1853a). Although not figured in the initial publication, Wagner later illustrated some of the teeth (Wagner, 1853b). The most detailed illustrations of the holotype specimen

were provided by Bauer (1898), including parts of the jaws and quadrate. The holotype material was destroyed during WWII; only thin sections of the teeth survive (Scheyer and Moser, 2011). A neotype for *I. leptospondylus* was selected by Bardet and Fernández (2000) from the Schwegler Museum (Langenaltheim, Bavaria, Germany), and was assigned to a new genus, *Aegirosaurus*. The neotype remained in Langenaltheim following the death of Mr. Schwegler, but is not publicly accessible. However, a cast of the skull is available in the collections of the SNSB-BSPG. The *A. leptospondylus* neotype and the holotype were considered to be different species by Maisch (2015) based on supposed differences in humeral morphology; however, the humerus of the holotype was not preserved (Wagner, 1853a; Bauer, 1898).

Following his initial description, Wagner (1861) referred a second specimen (the Häberlein specimen) to '*Ichthyosaurus' leptospondylus;* this material was also destroyed during WWII but is not considered to be congeneric with the holotype by more recent authors (Bardet and Fernández, 2000). Bardet and Fernández (2000) referred an additional post-war specimen to *A. leptospondylus*, SNSB-BSPG 1954 I 608. Some authors (Maisch and Matzke, 2000; Maisch, 2015) find this specimen to be inconsistent with the neotype, and Maisch (2015) specifically considered it to be closer to Wagner's conception of *A. leptospondylus*, i.e., the holotype. The enamel ornamentation has been described as differing between the holotype (ridged enamel in the holotype and neotype: Scheyer and Moser, 2011) and SNSB-BSPG 1954 I 608 (smooth enamel: Bardet and Fernández, 2000), as has the configuration of the distal facets on the humerus (Maisch, 2015). Two additional skulls, SMNS 54067 and NHMUK PV OR 42833, have also been referred to *A. leptospondylus* (Meyer, 1863; Bardet and Fernández, 2000; Maisch and Matzke, 2000); this material will be re-evaluated and discussed in more detail below.

In addition to the material referred to *Aegirosaurus leptospondylus*, Delsett et al. (2022) referred JME-SOS-08369, from the early Tithonian of Blumenberg, Germany, to *Aegirosaurus* sp.. They did not refer the material to *A. leptospondylus* due to the relatively long exposure of the maxilla (30% of snout length/40% if the suborbital portion of the maxilla is included in the measurement), somewhat longer than the values reported for material referred to *A. leptospondylus* (22% of snout length: SNSB-BSPG 1954 I 608; 25%: neotype (Bardet and Fernández, 2000); 27%: SMNS 54067).

From elsewhere in the world, Maisch and Matzke (2000) referred an ophthalmosaurine ichthyosaur from the Tithonian of Argentina to *Aegirosaurus*; however, this specimen is now considered to be distinct at the generic level (holotype of *Catutosaurus gaspariniae:* Fernández et al., 2021). Likewise, additional material from the Los Catutos Member of the Vaca Muerta Formation referred to *Aegirosaurus* by Gasparini et al. (2015) has since been determined to be generically distinct (holotype of *Sumpalla argentina*: Campos et al., 2021a).

Lastly, Fischer et al. (2011) referred an isolated lower jaw from the Valanginian (Early Cretaceous) of France to *Aegirosaurus* sp. Here we consider this specimen to be referable to Ophthalmosauria indet., following Lukeneder et al. (2022). Therefore to date, material referred to *Aegirosaurus* is only definitively known from the Late Jurassic of Germany.

MATERIALS AND METHODS

Geology

The Plattenkalk deposits of southern Germany have a long history of commercial exploitation and fossil collecting, and have produced spectacular vertebrate material over more than 200 years including diverse chondrichthyan and actinopterygian fishes, turtles, squamates, thalattosuchian crocodylomorphs, dinosaurs, and early birds (Arratia et al., 2015). Ichthyosaurs are a rare component of the fauna, although the number of specimens held in private collections exceeds publicly available materials. The specimens discussed here originate from the Middle Franconian Alb localities around Solnhofen (Apfelthal), Langenaltheim, Eichstätt, and Painten (Figure 1). All four localities are Late Jurassic in age, and consist of fine-grained, laminated, and planar limestones, usually lacking bioturbation (Viohl, 2015a). The Bavarian plattenkalk deposits formerly part of the "Weissjura" (Quenstedt, 1856-1858), including the localities mentioned above, are now divided into several different formations, ranging in age from the Kimmeridgian to Tithonian (Schweigert, 2007; Niebuhr and Pürner, 2014). We assigned ammonite zonation biostratigraphic ages to historical localities based on Schweigert (2007). During the Late Jurassic, this part of southern Germany was situated in a shallow tropical sea, with the laminated limestones being deposited in inter-reef basins (Viohl, 2015b).

FIGURE 1. Map of Late Jurassic Bavarian Plattenkalk localities discussed in the text (modified from Fürsich et al., 2007).

Materials

SM. The neotype of *Aegirosaurus leptospondylus* is a small, three-dimensionally preserved skeleton 1.77 m in length, including some soft tissue remains from the fore- and hind limbs, and the caudal fin. The skeleton has been exposed in dorsal view (Bardet and Fernández, 2000). As the original skeleton was not available for study, all observations were made on a cast of the skull housed at the SNSB-BSPG, Munich, resulting in uncertainty regarding the position of some of the cranial sutures. Since the interpretations of Bardet and Fernández (2000, fig. 3) were found to be generally reliable where these could be confidently checked against the cast, we describe only those points where a) additional detail was both visible on the cast and important for comparison, and b) those few cases where our interpretations differed from those Bardet and Fernández (2000) (see Appendix 1 for details). SM originates from Langenaltheim, Bavaria, Germany, from the Altmühltal Formation, Rueppellianus Subzone, Hybonotum Zone, lower Tithonian.

SNSB-BSPG 1954 I 608. This specimen was described in detail by Bardet and Fernández (2000), but also corresponds to 'Munich 5' of McGowan (1976). SNSB-BSPG 1954 I 608 is a small individual (79.3 cm preserved length) exposed in left lateral view; a counterpart is also available. The caudal region is missing; the posterior body and extremities are somewhat disarticulated. The skeleton is surrounded by numerous *Saccoccoma* remains. Although not noted in previous descriptions, an outline of the soft tissue hind fin is preserved. SNSB-BSPG 1954 I 608 originates from Geisberg quarry, Apfelthal, Mörnsheim, Bavaria, in the Altmühltal Formation, Rueppellianus Subzone, Hybonotum Zone, lower Tithonian.

SMNS 54067. This specimen was acquired by the SMNS in 1985. SMNS 54067 is a laterally compressed skull and the anterior part of the torso with shattered vertebrae and rib fragments, exposed from the left-hand side. The skull is well preserved except for the narial region and the posterodorsal portion of the skull. This specimen was noted by Maisch and Matzke (2000), but figured only as a reconstruction created by combining observations with SNSB-BSPG 1954 I 608. SMNS 54067 preserves indeterminate soft tissue remains in the anterior dorsal region. The specimen originates from Painten, Bavaria, from the Torleite Formation, Ulmense Subzone, Beckeri Zone, upper Kimmeridgian.

JME-SOS-08369. JME-SOS-08369 is an articulated ichthyosaur 1.84 m in total length, and includes a complete soft tissue envelope. This 'mummified' type of preservation unfortunately hides many osteological details due to low contrast with the surrounding soft tissues and soft tissue remains directly covering the bones. The specimen was described and figured by Delsett et al. (2022). JME-SOS-08369 originates from Blumenberg, Eichstätt, Bavaria, from the Altmühltal Formation, Riedense Subzone, Hybonotum Zone, lower Tithonian.

NHMUK PV OR 42833. NHMUK PV OR 42833 preserves the snout of a small ichthyosaur in dorsal view. The specimen has been dorsoventrally compacted. Originally described and figured by Meyer (1863), NHMUK PV OR 42833 was also described by Bardet and Fernández (2000). It originates from Eichstätt, Bavaria, from the Altmühltal Formation, Riedense Subzone, Hybonotum Zone, lower Tithonian.

Documentation

In addition to being photographed under natural light, SMNS 54067, SNSB-BSPG 1954 I 608 and NHMUK PV OR 42833 were photographed under UV-light. Depending on the material and wavelength, the fluorescence response differs and therefore is suited to distinguish the anatomical structures from the surrounding matrix. During photography of SMNS 54067, the three UV types were

tested independently from each other (photo with only UV-A; UV-B; UV-C) but also in combination (photos with UV-A/UV-C; UV-B/UV-C, UV-A/-B/-C). The UV analysis on SMNS 54067 was performed with a 95 W triple wavelength discharge lamp from WayTooCoolLLC; pictures were taken with a Canon 700D with either a 24, 50 and 100 mm lenses, of which the 24 and 50 mm were coupled with orange correction filters to counteract the blue halo from the bulbs. SNSB-BSPG 1954 I 608 and NHMUK PV OR 42833 were photographed with a hand-held LED UV torch (Alonefire SV83) emitting UV-A radiation (365 nm) with a Canon 200D. Unfortunately, SNSB-BSPG 1954 I 608 had been treated with a synthetic coating that masked soft-tissue structures under UV light.

Phylogenetic Analysis

To examine the position of *Aegirosaurus* and *Jabalisaurus tethyensis* sp. nov. in a phylogenetic context, we rescored *Aegirosaurus* in the matrix of Campos et al. (2025) based only on the neotype specimen, and also added *J. tethyensis* as an OTU. We removed *Muiscasaurus catheti* since in the matrix of Campos et al. this OTU is scored based on both the holotype and referred specimens (Maxwell et al., 2016; Páramo-Fonseca et al., 2021), which we do not consider to be congeneric. In addition, we updated the scoring of braincase characters for *Baptanodon natans* based on Massare and Connely (2022), as well as some cranial characters in *J. meztli* (see Appendix 2 for details). Scoring for humeral midshaft constriction was edited to '?' in *Catutosaurus gaspariniae* and was also scored as '?' for *J. tethyensis* because this character is known to be ontogenetically influenced (see Johnson, 1977: pl. 2), and the adult morphology is unknown in these OTUs.

In addition to these OTU-specific modifications, we reversed the character state descriptions for Ch. 9 (length of premaxillary process of the maxilla) to reflect existing scoring. We reformulated Ch. 15 (complete division of external nares) to eliminate the absence state, since in its previous formulation, it duplicated Ch. 14: state 3. Taxa in which a complete division was absent were scored as inapplicable ('-'). We also rescored Ch. 117 (postaxial enlargement of forefin) following Lomax et al. (2025) due to homology inconsistencies between authors focusing on ophthalmosaurian vs. non-ophthalmosaurian parvipelvians. We deleted Ch. 122 ("digital bifurcation in digit IV"). This character referred to the presence of interdigital ossicles between digits IV and V, which are known to vary both intraspecifically and asymmetrically within an individual (see Maxwell, 2012 for homology discussion). As scored, the 'present' state comprised interdigital ossicles between digits IV and V, true instances of digital bifurcation (e.g., some specimens of *Ichthyosaurus*: Motani [1999a]) and interdigital ossicles in the anterior limb (e.g., Kolb and Sander, 2009). Due to the high levels of intraspecific and intra-individual variation, this character was deleted rather than rescored or restructured.

These changes resulted in a matrix of 55 taxa and 130 characters, all of which were treated as unordered (Appendix 3). This matrix was analyzed in TnT v. 1.6 (Goloboff and Morales, 2023), using four optimization strategies: equal weights parsimony, and implied weights parsimony (k= 6, 9, 12). A new technology search was implemented using 50 iterations of the ratchet algorithm, recovering minimum length 50 times.

SYSTEMATIC PALAEONTOLOGY

ICHTHYOSAURIA de Blainville, 1835
OPHTHALMOSAURIA Motani, 1999b
PLATYPTERYGIINAE sensu Fischer et al., 2012
AEGIROSAURUS Bardet and Fernández, 2000

Type species. *Aegirosaurus leptospondylus* (Wagner, 1853a).

Diagnosis. As for type and only species.

Aegirosaurus leptospondylus (Wagner, 1853a)
Figure 2

Neotype. SM, a small, three-dimensional skeleton exposed in dorsal view.

Neotype locality and horizon. Langenaltheim, Bavaria; Altmühltal Formation, Rueppellianus Subzone, Hybonotum Zone, lower Tithonian.

Diagnosis (modified from Bardet and Fernández, 2000). A medium-sized ichthyosaur less than 2 m long, characterized by characterized by the following combination of character states: an extremely long and slender snout (snout ratio 0.73, similar to *Brachypterygius*), not markedly demarcated from the skull (unlike in e.g., *Baptanodon*); medium-sized orbit (orbital ratio 0.18, as in *Brachypterygius*); postorbital segment of the skull narrow (postorbital ratio 0.08); premaxillae comprising 63% of the skull in dorsal view; dorsoventrally deep maxilla (as in *Platypterygius australis*); prefrontal excluded from external nares (as in *Brachypterygius*, but unlike in *Thalassodraco*); rounded, undivided external narial opening (unlike in *Parrasaurus*); short, dorsoventrally compressed

FIGURE 2. Cast of the *Aegirosaurus leptospondylus* neotype (SNSB-BSPG). A, skull in right lateral view; B, premaxillary dentition showing coarsely ridged enamel; C, skull in dorsal view; D, interpretation of narial region in lateral view; E, interpretation of skull roof. Abbreviations: an, angular; de, dentary; f, frontal; j, jugal; lac, lacrimal; mx, maxilla; na, nasal; pa, parietal; pmx, premaxilla; pof, postfrontal; prf, prefrontal; sa, surangular; sq, squamosal; st, supratemporal.

jugal slightly exceeding the anterior orbital margin; postorbital covering quadratojugal; presence in the cheek region of a reduced, triangular and laterally exposed squamosal (unlike in *Caypullisaurus,* in which the squamosal is rectangular, or *Eternauta*, in which it is absent); rectangular parietals with long interparietal suture (unlike in *Palvennia, Janusaurus, Jabalisaurus*); frontals mediolaterally broad with small temporal process (unlike in *Palvennia*, in which the temporal process is absent); external exposure of postfrontal greatly reduced, almost or entirely excluded from participation in the supratemporal fenestra (as in *Leninia*); angular largely exposed laterally reaching as far anteriorly as the surangular; surangular fossa greatly reduced in depth and anteroposterior length (as in *Brachypterygius*); acutely pointed teeth with enamel crown ornamented with pronounced apicobasal ridges (density = 8–10/5 mm, unlike in *Thalassodraco* and *Catutosaurus* in which the enamel is smooth, and unlike in *Jabalisaurus* in which the enamel ridges are much finer and more densely spaced); forelimb with massive humerus bearing three distal articulations for radius, intermedium (the smallest) and ulna (as in *Brachypterygius* but unlike in all other Jurassic ophthalmosaurians); an extrazeugopodial element and associated digit distal to the radius (unlike in *Brachypterygius*, in which the extrazeugopodial element is anterior to the radius); six digits of which the fourth is the longest and comprises 23 elements; short hind limb with massive femur half the length of the humerus, articulating distally with two elements, and four digits (unlike in *Sumpalla*, in which the femur has three distal facets); both paddles composed of proximally packed polygonal elements becoming more widely spaced and rounded distally (unlike in *Baptanodon, Arthropterygius, Palvennia, Janusaurus* in which the limb elements are rounded).

Remarks. See Appendix 1 for a brief cranial description based on the SNSB-BSPG cast (Figure 2). We do not consider any of the previously referred specimens to be consistent with the neotype of *Aegirosaurus leptospondylus*.

ICHTHYOSAURIA de Blainville, 1835
OPHTHALMOSAURIA Motani, 1999b
OPHTHALMOSAURINAE sensu Fischer et al., 2012
JABALISAURUS Barrientos-Lara and Alvarado-Ortega, 2021a

Type species. *Jabalisaurus meztli* Barrientos-Lara and Alvarado-Ortega, 2021a.

Diagnosis (modified from Barrientos-Lara and Alvarado-Ortega, 2021a). A mid-sized ophthalmosaurian ichthyosaur ~2.0–3.2 m in length characterized by the following combination of character states: large orbit (orbital ratio ≥0.23, similar to *Ophthalmosaurus*); frontals medially elongate; parietals with short interparietal suture (as in *Palvennia*, *Janusaurus*, but differing from *Aegirosaurus*); postorbital crescentic, large, deeper than long, covering more than two-thirds of the cheek region (as in *Aegirosaurus*); snout slender (snout depth ratio < 0.045, as in *Acamptonectes*); external nares bilobate (as in *Baptanodon, Ophthalmosaurus* but differing from *Aegirosaurus*); distal end of humerus with three articular facets for the radius, ulna, and a preaxial element (as in *Baptanodon, Ophthalmosaurus* but differing from *Aegirosaurus*); manual phalanges polygonal (unlike in *Baptanodon, Ophthalmosaurus*).

Remarks. Many aspects of the cranial morphology of the holotype of *Jabalisaurus meztli* appear to be taphonomically influenced by head-first seafloor arrival and ssubsequent telescoping and differential compaction (see Wahl, 2009; Johnson et al., 2025), or are likely to have been misinterpreted due to said damage (especially in the narial region and skull roof); these characters have been excluded from our modified diagnosis. In general, *Jabalisaurus meztli* shows strong morphological similarities in skull proportions and anatomy to *Ophthalmosaurus* and *Baptanodon* (Gilmore, 1905; Moon and Kirton, 2016), differing most notably in the presence of tightly packed polygonal phalanges, and also in the extensive contribution of the splenial to the mandibular symphysis (Barrientos-Lara and Alvarado-Ortega, 2021a). The maximum body size estimate for the genus is based on the proportions of JME-SOS-08369 (see below) applied to the *J. meztli* holotype.

Jabalisaurus tethyensis sp. nov.
Figures 3–10

zoobank.org/A31C8BAC-80F4-4261-B042-5D2901E89DD0

v. 1976 *Ichthyosaurus*? *leptospondylus*? Wagner; McGowan (as Munich 5), p. 669.

v. 1978 *Ichthyosaurus (Macropterygius) posthumus* Wagner; Barthel, colour pl. 8 fig. 1.

v. 1990 *Macropterygius posthumus* (Wagner); Barthel et al., fig. 7.74.

vp. 2000 *Aegirosaurus leptospondylus* (Wagner); Bardet and Fernández, figs 2, 4, 7.

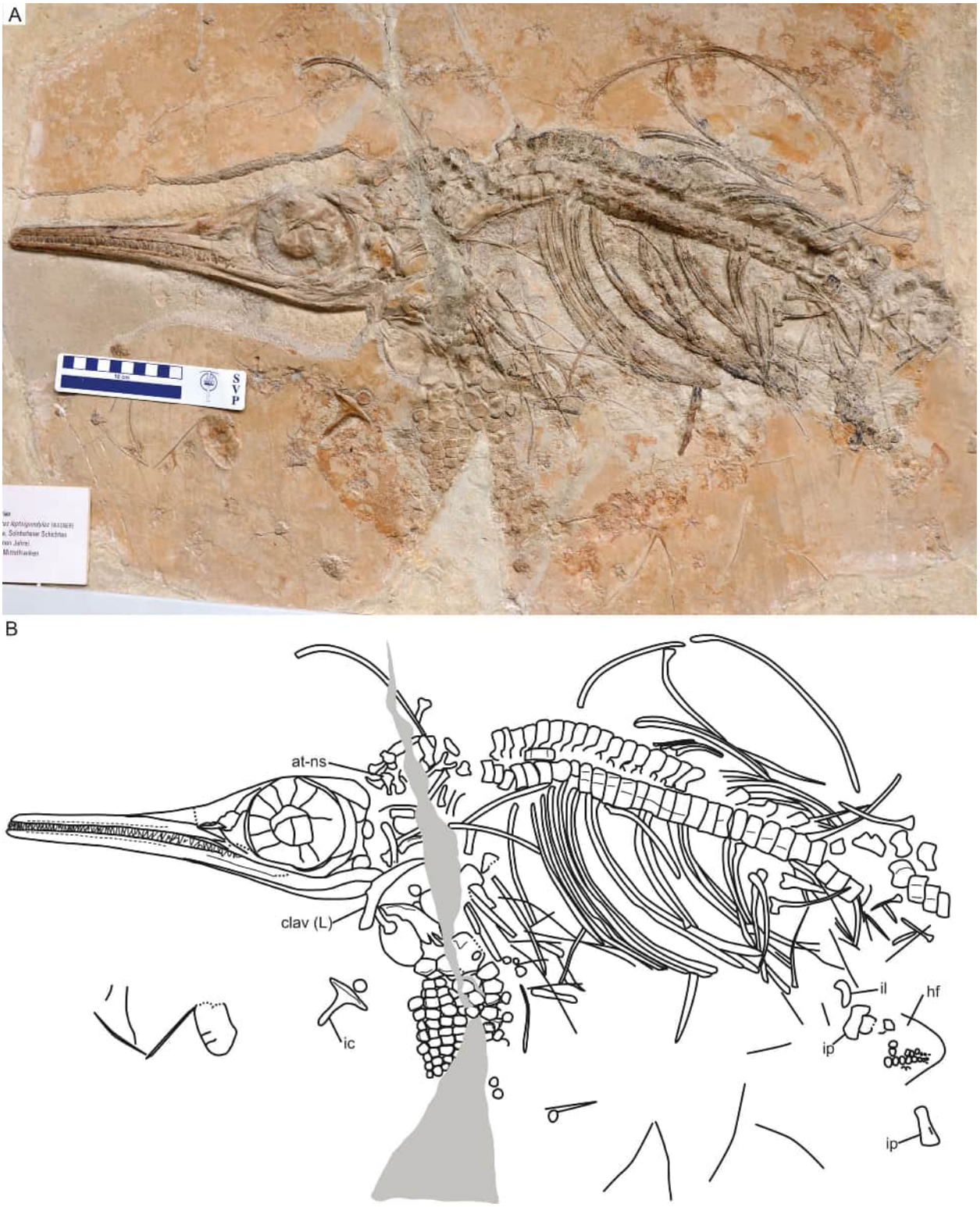

FIGURE 3. *Jabalisaurus tethyensis*, holotype specimen SNSB-BSPG 1954 I 608. A, overview photo; B, interpretive drawing. Abbreviations. at-ns, atlas neural spine; clav (L), left clavicle; hf, hind fin; ic, interclavicle; il, ilium; ip, ischio-pubis.

vp. 2000 *Aegirosaurus leptospondylus* (Wagner); Maisch and Matzke, fig. 8.

v. 2022 *Aegirosaurus* sp.; Delsett et al., figs 2, 5–7.

vp. 2022 *Aegirosaurus*? sp.; Serafini et al., p. 10, table 1.

Holotype. SNSB-BSPG 1954 I 608, a small juvenile (osteologically immature) individual preserved as part and counterpart (Figures 3–6).

Etymology. The specific epithet refers to the palaeogeographical distribution of this species along the northern Tethyan shelf.

Type locality and horizon. Geisberg quarry, Apfelthal, Mörnsheim, Bavaria. Altmühltal Formation, Rueppellianus Subzone, Hybonotum Zone, lower Tithonian.

Diagnosis. A mid-sized ophthalmosaurian estimated at 2.0–2.9 m total length (upper limit calculated based on a neonatal/maternal skull length ratio of 45% for *Stenopterygius*, with total length extrapolated from skull length using proportions of JME-SOS-08369) and differing from the type species based on a reduced contribution of the splenial to the mandibular symphysis (<50%; assessed based on JME-SOS-08369, vs. 60% in *J. meztli*). The following character states differentiate *Jabalisaurus tethyensis* from all other ophthalmosaurians: High-crowned skull with slender snout and short postorbital region; participation of prefrontal in posterodorsal external narial opening (as in *Ophthalmosaurus* and *Thalassodraco* but unlike in *Aegirosaurus*); bilobate external nares; triangular squamosal (unlike in *Caypullisaurus*); surangular fossa bordered dorsally by sharp crest (unlike in *Aegirosaurus, Brachypterygius*); delicate teeth, enamel ornamented with fine apicobasal ridges (density ~17–18/5 mm, unlike in *Thalassodraco* and *Catutosaurus* in which the enamel is smooth); humerus with three distal facets for the radius, ulna, and preaxial element (unlike in *Aegirosaurus, Brachypterygius* in which the middle facet articulates with the intermedium); tightly packed polygonal phalanges (unlike in *Baptanodon, Ophthalmosaurus*); bipartite pelvic girdle with completely fused, plate-like ischiopubis retaining the obturator foramen (unlike in *Undorosaurus* and *Thalassodraco* in which the ischium and pubis are medially separate, and also differing from *Caypullisaurus* and *Janusaurus* in which the obturator foramen has been lost). In overall morphology, *Jabalisaurus tethyensis* resembles *Ophthalmosaurus icenicus*, but differs in forefin anatomy distal to the humerus.

Referred specimens. SMNS 54067, JME-SOS-08369.

Locality and horizon (referred specimens). SMNS 54067, Torleite Formation, Painten, Bavaria, Ulmense Subzone, Beckeri Zone, upper Kimmeridgian; JME-SOS-08369, Altmühltal Formation, Blumenberg, Eichstätt, Riedense Subzone, Hybonotum Zone, lower Tithonian.

Remarks. The holotype and both referred specimens are consistent with a single taxon based on similar cranial shape and proportions, dentition, visible cranial anatomy consistent with *Ophthalmosaurus*, in combination with polygonal phalanges in the forelimbs (in SNSB-BSPG 1954 I 608 and JME-SOS-08369). Thus, while the three specimens are not characterized by any unambiguous features conclusively uniting them as a single taxon, overall anatomical similarities as well as similar geographic and temporal provenance suggest that they are conspecific. The features uniting these three specimens are inconsistent with *Aegirosaurus leptospondylus*, the only other named ichthyosaur taxon from the Bavarian Plattenkalk deposits. While at least two additional taxa were likely present in the Late Jurassic of Germany, these are differentiated from *Jabalisaurus tethyensis* by relative tooth size and cranial proportions, with both the undescribed taxa being much more robust and with larger teeth. Thus, the most parsimonious hypothesis is that SNSB-BSPG 1954 I 608, SMNS 54067, and JME-SOS-08369 represent a single taxon. However, in case this conclusion becomes unjustified in the future, we base the description and diagnosis on the holotype specimen SNSB-BSPG 1954 I 608 unless otherwise noted.

Despite its immature ontogenetic stage, SNSB-BSPG 1954 I 608 was selected as the holotype of *Jabalisaurus tethyensis* since it is by far the most complete specimen of the three in terms of the amount of anatomical detail visible.

Description

Based on holotype specimen SNSB-BSPG 1954 I 608 unless otherwise noted.

General observations. The holotype specimen is a very young juvenile, preserved in lateral view (Figure 3). The snout ratio = 0.62 (referred specimens both = 0.65; Table 1), and the skull is high-crowned, although appears lower due to damage to the dorsal orbit. The orbit is completely filled by the scleral ring, and is rather large (orbital ratio = 0.26; referred specimens = 0.23–0.26). Despite the much smaller size of SNSB-BSPG 1954 I 608, both

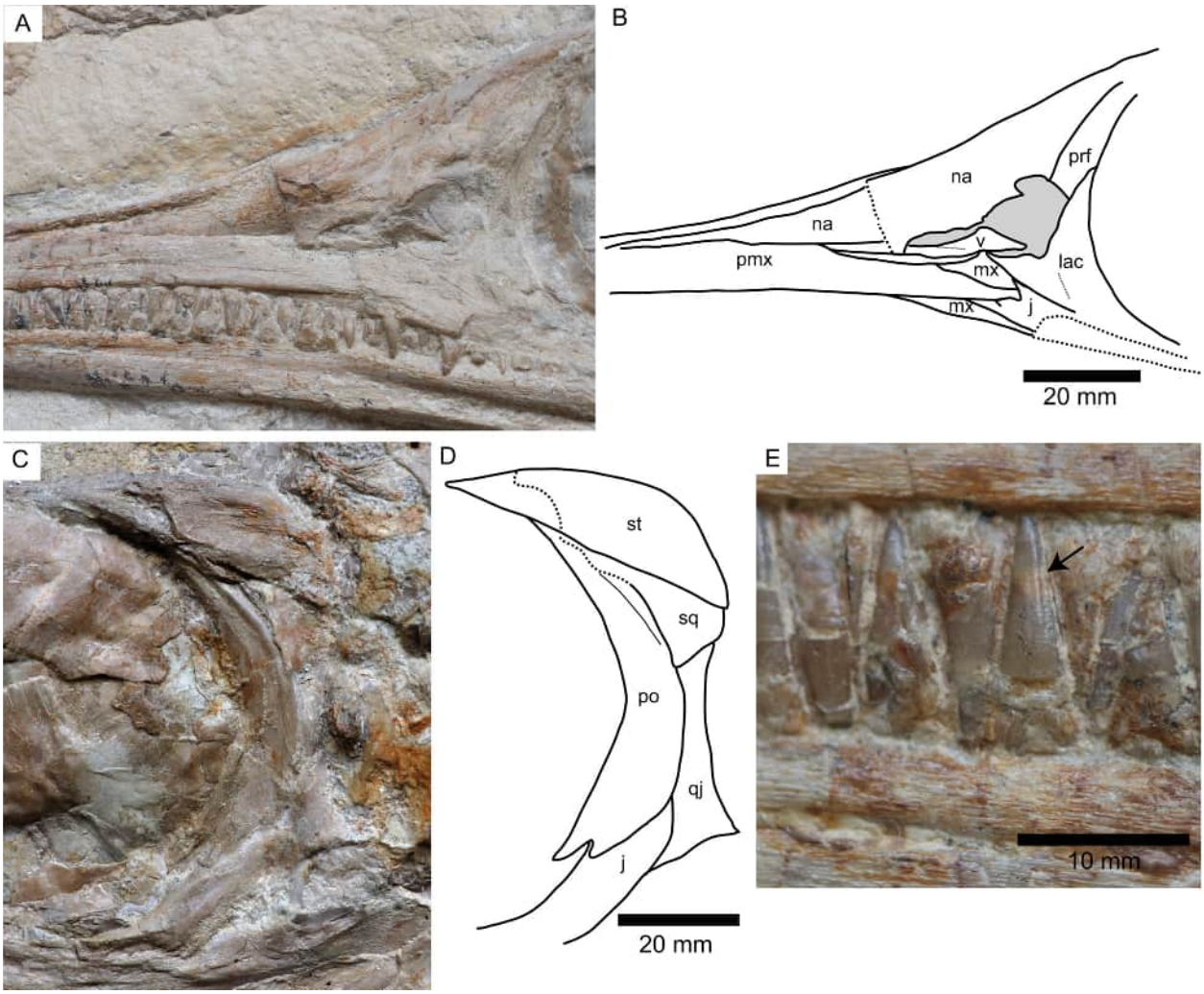

FIGURE 4. *Jabalisaurus tethyensis*, holotype specimen SNSB-BSPG 1954 I 608. A, photo and B, interpretation of narial region; C, photo, and D, interpretation of cheek region; E, close-up of dentition from near the mid-point of the snout showing the absence of a distinct enamel layer and the faint ridging of the underlying dentine (arrow). Abbreviations: j, jugal; lac, lacrimal; mx, maxilla; na, nasal; pmx, premaxilla; po, postorbital; qj, quadratojugal; sq, squamosal; st, supratemporal; v, vomer.

the external diameter and aperture of the scleral ring are larger than in the *Aegirosaurus leptospondylus* neotype. The narial opening is clearly bilobate, separated by a robust descending process of the nasal and a small ascending process of the maxilla (Figure 4A, B).

Premaxilla. The premaxilla has greatly reduced dorsal exposure relative to the *Aegirosaurus* neotype, composing just over 1/2 (52%) of the snout (vs. 48% nasal), and 45-48% of the lateral surface relative to the maxilla (vs. 55% premaxillary ratio in the *Aegirosaurus* neotype). As with the neotype, the premaxillary fossa is present but discontinuous. The dorsal premaxilla is broken immediately anterior to the narial opening; UV photography indicates that the bone fragment identified as the supranarial process by Bardet and Fernández (2000) is part of the underlying nasal. The subnarial process of the premaxilla contacts the anterior jugal posteriorly (Figure 4A, B). The lacrimal appears to be excluded from contact with the premaxilla. The snout is very slender in all three skulls, but appears most slender in JME-SOS-08369 (Figure 9B). However, the dorsal surface of the latter skull appears to still be partially embedded in matrix, exaggerating the slenderness of the rostrum.

In SMNS 54067, the anteriormost premaxillae do not contact each other medially and are rather pointed anteriorly.

FIGURE 5. *Jabalisaurus tethyensis*, holotype specimen SNSB-BSPG 1954 I 608, pectoral girdle. A, interclavicle in ventral view; B, pectoral girdle and proximal forelimb (part); C, left humerus (counterpart). Abbreviations. clav (R), right clavicle; cor (L?), presumed left coracoid; dp, dorsal process; H (L), left humerus; paf, preaxial facet; R, radius, Rf, radial facet; ri, rib; scap (L), left scapula, U, ulna, UF, ulnar facet.

Maxilla. The maxilla has limited exposure laterally, being very short anteriorly (barely exceeding the external nares in length) and laterally covered by the jugal posteriorly and premaxilla anteriorly (Figure 4A, B). There is a small lateral exposure of the maxilla ventral to the anterior external nares and anterior to the lacrimal, the posterior edge of which forms a small dorsal process that does not contact the descending process of the nasal. Approximately 16 maxillary tooth positions are present (vs. 12: McGowan, 1976), with the difference in count likely due to the suborbital tooth positions that were difficult to differentiate under natural light.

Delsett et al. (2022) noted differences in maxillary morphology between JME-SOS-08369 and SNSB-BSPG 1954 I 608. These include a proportionately longer maxilla in JME-SOS-08369 relative to the external narial opening (but not relative to the premaxilla; see premaxillary ratios in Table 1). This difference is attributed to dorsoventral compaction of the snout, resulting in the concealment of the anterior lobe of the external narial opening in JME-SOS-08369. JME-SOS-08369 has ca. 21 maxillary tooth positions/18 teeth preserved (vs. 16: SNSB-BSPG 1954 I 608).

SMNS 54067 has ~23 maxillary tooth positions, a much higher count than SNSB-BSPG 1954 I 608. This skull also has the lowest premaxillary ratio (=0.45), indicating that a proportionately longer maxilla could be responsible for the higher maxillary tooth count; however an increase in the number of tooth positions with increasing jaw length is also possible, and may also explain the

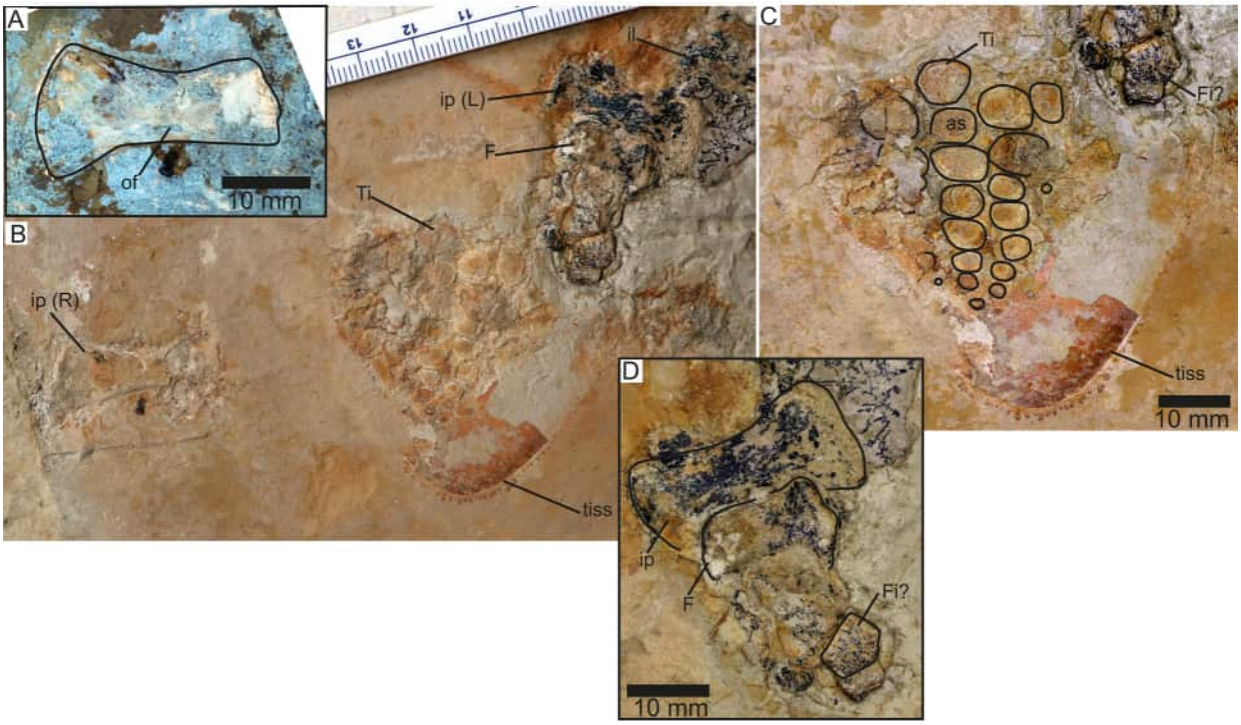

FIGURE 6. *Jabalisaurus tethyensis*, holotype specimen SNSB-BSPG 1954 I 608, pelvic girdle. A, right ischiopubis under UV-A light, the blue film is the remains of a synthetic coating; B, pelvic girdle and hind limb under natural light; C, hind fin and associated soft tissue envelope. Note the persistence of dendrites around the outline of the fin where the soft tissue itself has flaked off. D, close-up of femur and surrounding elements. Abbreviations. as, astragalus; F, femur; Fi, fibula; il, ilium; ip, ischiopubis; of, obturator foramen; Ti, tibia; tiss, soft tissue fin.

discrepancy between JME-SOS-08369 and SNSB-BSPG 1954 I 608. In both JME-SOS-08369 and SMNS 54067, the maxillary tooth row extends well under the orbit (Figures 7A–B, 9B), almost to the orbital mid-point; as noted above damage to the suborbital bar may be influencing this trait in SNSB-BSPG 1954 I 608.

Lacrimal. In SNSB-BSPG 1954 I 608, the lacrimal forms the posterior and ventral edges of the posterior external narial opening (Figure 4A–B). A poorly developed ridge is visible on the lateral surface of the orbital process of the element, likely representing the edge of the circumorbital area. The distance between the orbit and external nares is very short. The dorsal surface of the anterior process has a scalloped edge and is thickened. Dorsally, the lacrimal is excluded from contact with the nasal by the narial process of the prefrontal. Ventrally, the lacrimal contacts the jugal and maxilla in lateral view. The lacrimal does not contact the subnarial process of the premaxilla.

Vomer. The vomer is visible in the narial opening, pushed outward during compression of the skull (Figure 4A–B). The vomer is dorsoventrally expanded ventral to the descending process of the nasal. This expanded surface forms a concave choanal wall separated from the more anterior wall of the vestibulum nasi by a ridge. The morphology appears to be identical to that of *Ophthalmosaurus*, and differs notably from e.g., *Platypterygius australis*, in which the crest of the vomer forms two diverging processes (Kear, 2005; Moon and Kirton, 2016).

Nasal. The nasal forms the dorsal surface of 48% of the snout. The surface dorsal to the external nares forms three arches in lateral view: a low anterior one, a large, more steeply angled middle arch that forms a laterally projecting flange that descends into the narial opening, and a small, dorsally positioned posterior arch that also bulges slightly laterally and might represent a foramen. The nasal does not contact the lacrimal (Figure 4A–B).

SMNS 54067 preserves a portion of the skull roof, including the posterior nasals. A well-developed internarial depression is present; the internasal suture in this region appears to show extensive asymmetry. The nasals overlap the frontals posteriorly and posterolaterally and articulate with the prefrontal laterally (Figure 7A–E).

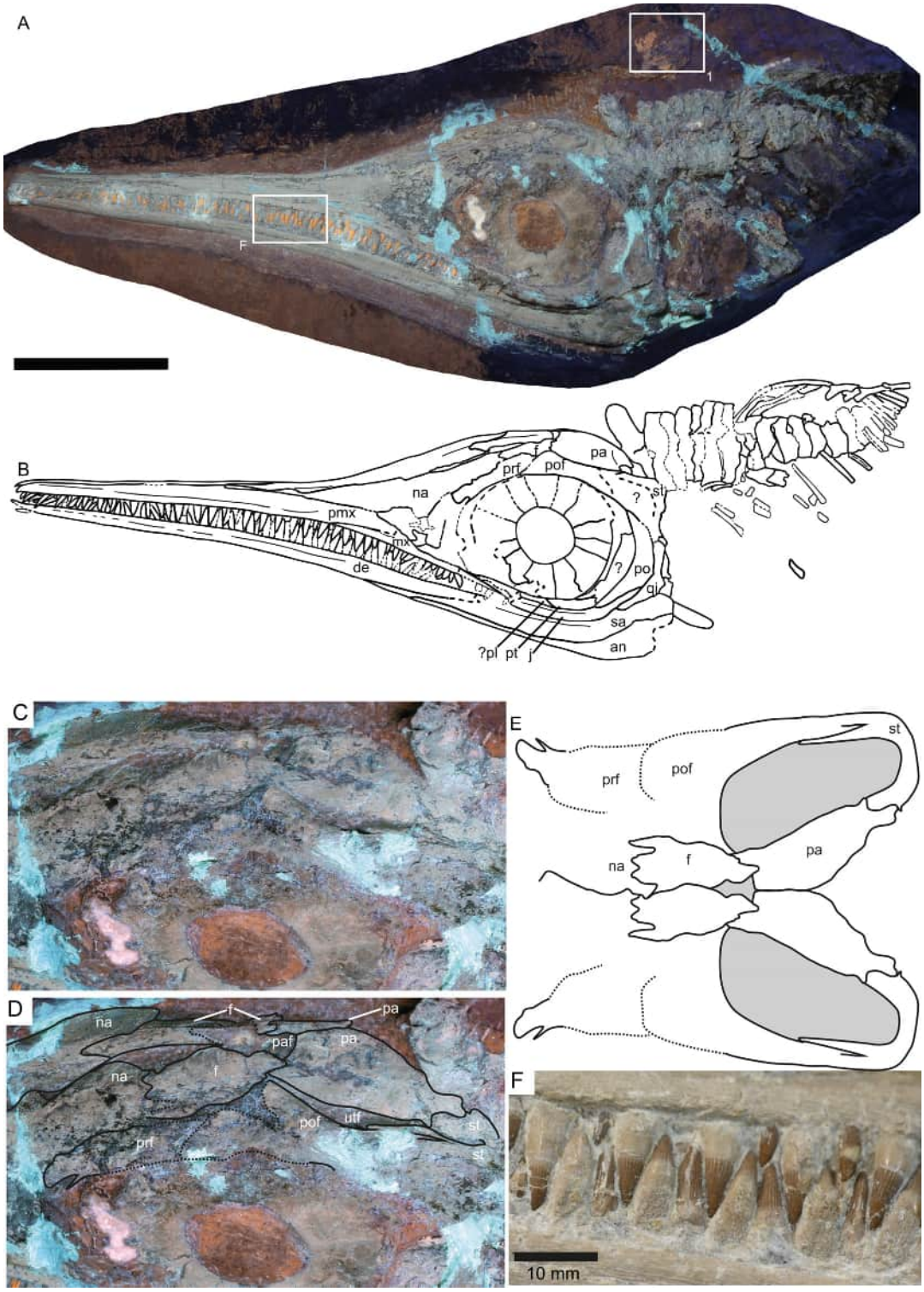

FIGURE 7. *Jabalisaurus tethyensis*, referred specimen SMNS 54067. A, overview under UV-ABC light, the inset box 1 indicates the location of the soft tissue structures illustrated in Figure 8; B, interpretive drawing; C, skull roof photographed under UV-AC; D, interpretive drawing; E, skull roof reconstruction. Note that due to strong lateral taphonomic compaction of the skull, the width of the temporal fenestrae is speculative. F, close-up of the dentition slightly posterior to the snout mid-point under natural light. Abbreviations. an, angular; de, dentary; f, frontal; j, jugal; mx, maxilla; na, nasal; pa, parietal; paf, parietal foramen; ?pl, palatine?; pmx, premaxilla; po, postorbital; pof, postfrontal; prf, prefrontal; pt, pterygoid; qj, quadratojugal; sa, surangular; st, supratemporal; utf, upper temporal fenestra.

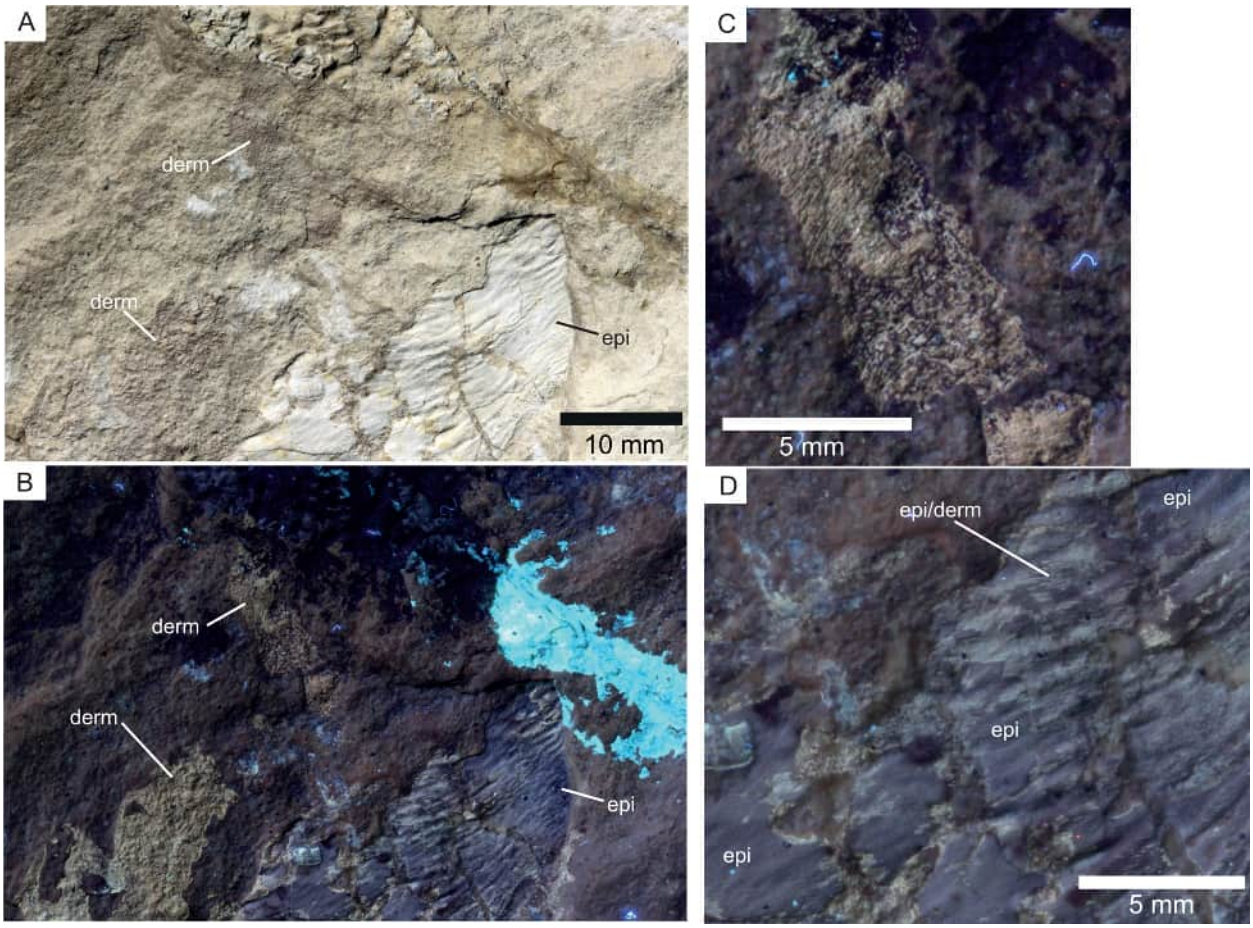

FIGURE 8. *Jabalisaurus tethyensis*, referred specimen SMNS 54067, soft tissues. A, preserved soft tissue remains under natural light; B, the same under UV-AC light; C, magnified view of the dermis showing the parallel ridged texture; D, magnified view of the epidermis showing the folded structure, darker-fluorescing epidermis, and the damaged patches where the ridged dermis is faintly visible underneath. Abbreviations. derm, dermis; epi, epidermis; epi/derm, areas where the epidermis is damaged and the underlying dermis is visible.

Prefrontal. The prefrontal makes up the anterior dorsal edge of the orbit, and sends a broad, poorly mineralized narial process ventrally to form the posterodorsal edge of the external narial opening (Figure 4A–B).

SMNS 54067 preserves the posterior portion of the prefrontal (Figure 7C-D). The prefrontal has a very small medial contact with the frontal and articulates with the postfrontal posteriorly. Evidence of damage to the superficial layer of bone in the region of the frontal-prefrontal articulation means that this contact may have been covered by the overlapping nasal in external view, as is the case in *Ophthalmosaurus icenicus* (Moon and Kirton, 2016).

Postfrontal. Only the posteriormost postfrontal is preserved in SNSB-BSPG 1954 I 608, overlapping the anterior ramus of the supratemporal on the lateral surface of the skull. A contact with the squamosal is small, if present at all in external view.

The postfrontal is also preserved in SMNS 54067, but has been extensively damaged. It makes up the anterior edge of the upper temporal fenestra, as well as the anterior portion of the lateral edge, and appears to have a small contact with the frontal anteromedially (Figure 7C–E). Posteriorly, the postfrontal articulates with the supratemporal, and posteroventrally with the postorbital. However, the superficial layer of bone has been removed in the lateral temporal region, making the relationships between the postfrontal and other elements difficult to distinguish in lateral view.

Frontal. The frontals are preserved only in SMNS 54067 (Figure 7C–E). The frontals are externally convex. Anteriorly, the internasal depression extends posteriorly onto the anterior frontals. The

FIGURE 9. *Jabalisaurus tethyensis*, referred specimen JME-SOS-08369. A, overview photograph, box 'G' indicates the location of the preserved gastric contents, arrowhead indicates location of ischiopubis (not easily visible under natural light); B, close-up of skull; C, close-up of dentition.

anterior right frontal is exposed in medial view; in this view it is evident that the frontals extend much further anteriorly under the nasals than is externally exposed. The left and right frontals enclose the anterior parietal foramen. The suture between the posterior frontals and the parietal is somewhat crenulated. The nasals overlap the frontals anteriorly.

Parietal. The parietals are preserved only in SMNS 54067 (Figure 7C–E). The right and left parietals remain in articulation along the interparietal suture, but only the left one is usefully exposed. The parietals form the posterior edge of the parietal foramen and anteriorly are overlapped laterally by the frontals. Posteriorly, the parietal shows a concave posterior edge well anterior to its articulation with the supratemporal. Based on this morphology, the length of the interparietal suture appears to have been very short, and the posterolateral process relatively long.

Postorbital. The postorbital is relatively broad, crescentic in shape (Figures 4C-D, 7A, B). The anterodorsal portion forms a transverse flange, as in *Ophthalmosaurus*, whereas the posterior and ventral components are laterally oriented.

FIGURE 10. *Jabalisaurus tethyensis*, referred specimen JME-SOS-08369. A, phalanges from the right forelimb, with arrow indicating polygonal morphology; B, phalanges from the left forelimb, also showing polygonal form. C, ischiopubis, photographed under UV-light.

Supratemporal. Only the posterolateral supratemporal is visible in SNSB-BSPG 1954 I 608; it has a broad exposure on the lateral surface of the cheek, articulating with the squamosal ventrally (Figure 4C–D).

In SMNS 54067, the supratemporal is also preserved (Figure 7A–D). Although somewhat damaged, some general observations can be made. The anterior ramus makes up most of the lateral edge of the upper temporal fenestra, with an elongate anteromedial process excluding the postfrontal from the posterolateral UTF, and a shorter lateral ramus. The medial ramus of the supratemporal forms an interdigitating suture with the posterolateral process of the parietal.

Squamosal. The squamosal is small, triangular, and laterally oriented (Figure 4C–D). It does not appear to reach the postfrontal anteriorly, but this region is not well preserved. Ventrally, the squamosal contacts the quadratojugal.

Quadratojugal. The dorsal portion of the quadratojugal is tall and narrow (Figures 4C–D; 7A–B). The ventral edge is elongate, extending almost as far anteriorly as the anteriormost postorbital, as in *Ophthalmosaurus icenicus* (Moon and Kirton, 2016). A small quadrate process is present.

Jugal. The dorsal ramus of the jugal is deeply bowed ventral to the postorbital (Figure 3); this is known to be ontogenetically influenced in other ichthyosaurs, related to larger eye size in small juveniles (Miedema and Maxwell, 2022), and this is also likely the case here. The dorsal ramus articulates with the postorbital anteriorly, and the quadratojugal posteriorly (Figures 4C–D, 7A–B). Anteriorly, the jugal extends well past the orbital margin and broadly covers the posterolateral maxilla to contact the subnarial process of the premax-

TABLE 1. Comparison of ratio characters (sensu McGowan, 1976) between the specimens discussed in the text. Specimens referred to *Jabalisaurus tethyensis* are shaded in grey.

Specimen	Lower jaw length (mm)	Snout ratio	Orbital ratio	Premaxillary ratio	Prenarial ratio	Snout depth ratio (x10)	Postorbital: orbital ratio***
Aegirosaurus leptospondylus neotype	565	0.73	0.18	0.55	0.67	~0.48	0.43
SNSB-BSPG 1954 I 608	314	0.62	0.26	0.48	0.51	~0.30	0.23
SMNS 54067	473	0.65	0.26	0.45	0.53	0.35	0.39
JME-SOS-08369	440	0.65	0.23	0.47	0.57	~0.20	--
NHMUK PV OR 42833	~353 **	0.71	--	0.48	0.59	--	--
Jabalisaurus meztli	750	0.67*	0.24	0.44*	0.52*	0.44	0.45

*calculated from the reconstruction presented in Barrientos-Lara and Alvarado-Ortega (2021a).
**Corrected estimate based on proportions in von Meyer (1863), completeness estimate of the anterior premaxilla revised.
*** Postorbital length compared to orbital length rather than jaw length to provide a comparison independent of snout elongation

illa (Figure 4A–B). The portion of the jugal ventral to the orbit is not preserved.

In SMNS 54067, the jugal is still deeply bowed ventral to the orbit but bears a small posterior heel (Figure 7A–B). The jugal is grooved along its lateral surface, both posteriorly (SMNS 54067) and anteriorly (JME-SOS-08369; Figure 9B).

Lower jaw. The angular has extensive exposure on the retroarticular process, but rapidly narrows anteriorly (Figures 3, 7A–B). The surangular fossa is well-developed. The dentary fossa begins as intermittent foramina anteriorly and becomes continuous more posteriorly.

The skull of JME-SOS-08369 is exposed in lateroventral view, thus exposing more of the ventral surface of the lower jaw (Figure 9B). This angle of preservation is the reason for the perceived larger angular exposure in this specimen than in the other two skulls. The angular and surangular extend approximately the same distance anteriorly, to a point just posterior to the mandibular symphysis. The splenial is exposed along the medial surface of the lower jaw, and makes up slightly less than half of the mandibular symphysis.

Dentition. Contrary to previous reports, enamel is likely not preserved in SNSB-BSPG 1954 I 608. This was assessed both in natural light and under UV, where differential fluorescence was only faintly developed in some of the maxillary teeth. However, the enamel was clearly ridged, based on faint scalloping of the external surface of the teeth when light was reflected off the dentine (Figure 4E). Enamel ridges appear to have extended from the tooth apex to the base of the enamel layer. Basal to the crown, the surface of the root is smooth and ungrooved. Tooth roots are round in cross-section.

SMNS 54067 has an exceptionally well-preserved dentition, with at least 57 teeth preserved in the upper and 39 teeth preserved in the lower jaw (Figure 7A–B, F). Enamel ridges occur at a density of 17–18/5 mm (Serafini et al., 2022), and are well developed at the crown base but become reduced or absent towards the apex. Heterodonty is pronounced, with posterior maxillary teeth being much shorter and blunter than the anterior dentition. The width at the crown base of the mid-premaxillary teeth is ca. 3.4 mm, becoming broader in the anterior maxillary teeth and narrower in the anteriormost teeth; crown height = 7.0 mm in the mid-premaxillary teeth, becoming reduced posteriorly. Tooth roots are oval in cross-section.

JME-SOS-08369 also shows densely ridged enamel, ca. 18 ridges/5 mm (Figure 9B–C). As in SMNS 54067, the posterior maxillary tooth crowns are much shorter and blunter than the anterior teeth. Tooth crowns in the mid-snout dentition are approximately 2.5 mm wide at the crown base, and crown height is ca. 5 mm.

Scleral ring. The scleral ring of SNSB-BSPG 1954 I 608 is composed of ~14 plates, and measures 79 x 68 mm externally and the aperture diameter is 34 x 32 mm.

The scleral ring in SMNS 54067 consists of 13 plates and measures 106 x 91 mm externally and the aperture diameter is 43 x 42 mm.

Postcranium

Axial skeleton. The anteriormost vertebral column is disarticulated, but beginning in the anterior dor-

sal region to the posterior dorsal region, the column is in articulation (Figure 3). The wide neural canal observed in SNSB-BSPG 1954 I 608 is likely ontogenetically influenced, caused by negative allometry of the central nervous system relative to the postcranium. The poorly defined di- and parapophyses on the lateral surfaces of the anterior dorsal centra, which are not separated by cortical bone from either each other, the articular face of the centrum or the neural arch facets are also indicative of a young ontogenetic stage.

The atlas-axis neural spines in SNSB-BSPG 1954 I 608 are preserved posterior to the skull. That of the atlas has notably more slender ventral pedicles than that of the axis, and a much shorter neural spine. A weak anterior bulge marks an incipient proatlas process. The atlas neural spine overlaps that of the axis posteriorly.

The anterior dorsal neural spines in SNSB-BSPG 1954 I 608 are capped by a layer of tissue separate from the spines themselves; this is interpreted as mineralizing cartilage at the growing end of the spine and differs in both position and texture from the structures described dorsal to the neural spines in *Stenopterygius* (McGowan, 1992).

The ribs in SNSB-BSPG 1954 I 608 bear prominent grooves along their anterior and posterior surfaces. As noted by Bardet and Fernández (2000), the tuberculum and capitulum of the ribs are confluent; i.e., the rib has two articular facets but is effectively unicipital (= sheathed bicapitate morphology). This is interpreted as resulting from the extreme osteological immaturity of the specimen, but this character has not been previously described as ontogenetically variable. Gastralia were present, preserved as slender, curved rods.

The anteriormost neural spine preserved in SMNS 54067 is greatly thickened distally. This is very different in morphology from that of the atlantal neural spine of SNSB-BSPG 1954 I 608, and the significance of this thickening is unclear. SMNS 54067 preserves ribs that are clearly bicipital, with broad separation between the capitulum and tuberculum in the anterior dorsal region.

The ribs of JME-SOS-08369 have also been described as bicipital (Delsett et al., 2022). The gastral basket in JME-SOS-08369 is complete and extensive, with the gastralia extending from the pectoral girdle to within ca. 5 centra of the pelvic girdle. A median gastral element is absent. JME-SOS-08369 preserves the complete vertebral column, although preservation makes detailed observations impossible (Figure 9A). Seventy postflexural centra are ossified (Delsett et al., 2022).

Pectoral girdle and forelimb. Of the girdle elements, the interclavicle is preserved in external view, displaced from the rest of the girdle (Figures 3, 5A). It is approximately T-shaped, although the transverse bar is anteriorly convex, and posteriorly is connected to the median stem via broad laminae. The thickened convex portion of the transverse bar projects ventrally relative to the rest of the interclavicle. The transverse bar is slightly longer than the median stem, and bears a ridge parallel to its anterior margin. The median stem is straight and not posteriorly expanded. A partial scapula (right) is preserved in external view; however, the anterior and posterior portions are separated by a broad crack making assessment of details difficult (Figure 3, 5B). The dorsal anterior portion is concave. Assuming the scapula remains in articulation with the coracoid: the coracoid is also from the right side and preserved in external view, and is mediolaterally/ anteroposteriorly equidimensional. The coracoid is partially overlain by the right clavicle; the left clavicle is preserved above. Medially, the clavicles are broad and sheet-like with interdigitating surfaces; laterally they narrow to thin spines. The internal surface at the point where the clavicles narrow is deeply grooved.

Both forelimbs are partially preserved and articulated. A humerus, interpreted as the left one based on the position of the process closer to the midline than to the anterior margin and therefore identified as the dorsal process, is exposed (Figures 3, 5B, C). The distal end of the humerus is damaged anteriorly on the main slab, but two concave facets are present: a larger one for the ulna and a smaller anterior facet for the radius. The facets are clearly offset. A large preaxial facet is visible on the counterpart (Figure 5C). The distal end of the humerus is wider than the proximal end on the main slab, but on the counterslab, it appears that the proximal end is also quite wide, giving the humerus a short, squat shape as is typical for very young individuals. The humerus does not appear to be strongly waisted at the midpoint, but this might also be an ontogenetically dependent character (Johnson, 1977). Proximally, a protruding triangular dorsal process is present, angled anteriorly and situated nearer to the midline of the humerus than to the anterior edge. The crest does not reach the proximodistal midpoint of the humerus.

Both ulnae are preserved, although that on the right is damaged posteriorly (Figures 3, 5B). The ulna has six sides, the smallest being the ante-

rior surface for articulation with the radius. It is unclear if the posterior surface of the ulna was covered in cortical bone; however this trait is expected to be ontogenetically influenced so absence in this individual is not conclusive of the state in the taxon (Maxwell et al., 2014). The radius is pentagonal. The intermedium, while not preserved, would have articulated between the radius and ulna. The left forelimb is disrupted, with a block of six elements oriented distal-to-proximal directly below the radius and ulna. These are assumed to have been displaced from the right limb. Phalanges are generally tightly packed and rectangular in shape, becoming more rounded at the periphery of the fin.

The phalanges in JME-SOS-08369 were previously described as rounded (Delsett et al., 2022); however, numerous polygonal phalanges are visible on this specimen (Figure 10A–B).

Pelvic girdle. Both ischiopubes and both ilia are preserved in SNSB-BSPG 1954 I 608 (Figures 3, 6A–C). The right ischiopubis has been somewhat displaced and is exposed in lateral view (Figure 6A–B); based on this interpretation the left ischiopubis (Figure 6C) is also exposed in lateral view. Bardet and Fernández (2000) interpreted an obturator foramen as absent; Maisch and Matzke (2000, fig. 32) assumed this foramen was present but could not observe it directly. Under UV light, a foramen appears to be present (Figure 6A). The ischiopubis is fully fused and plate-like, measuring 28 mm in length. The ilia are robust and comma-shaped, 23 mm in length.

An ischiopubis is also present in JME-SOS-08369, interpreted as the right and measuring 48 mm in length (Figure 10C). We interpret the ischiopubis as having flipped such that its internal surface is directed externally, and the anterior surface is facing posteriorly. This interpretation may seem implausible given the high degree of articulation of this specimen; however, the contralateral ischiopubis and hind limbs do not appear to be in articulation, indicating some disruption to the region. Moreover, the posteriorly facing edge of the ischiopubis is more consistent with the anterior edge of an ischiopubis based on morphology. No obturator foramen is visible; however, the posteriorly facing side of the element is damaged in a way suggestive of the pubis having been broken near the foramen. The medial (distal) edge is plate-like. Delsett et al. (2022) interpreted two straight, rod-like elements in the posterior abdominal region as ilia. These are morphologically distinct from the ilia of SNSB-BSPG 1954 I 608, which are strongly curved rather than straight. It seems likely that these elements have been misidentified, especially since the figured example (left) does not fluoresce in the same way as the other ossified elements under UV light (Delsett et al., 2022, fig. 6c).

Hind limb. The femur in SNSB-BSPG 1954 I 608 is much shorter than the ischiopubis (Figure 6B–C). Given its close association with the proximal ischiopubis, it is most likely to be the left femur, and the position of the trochanter indicates that it is exposed in dorsal view. Two distal articular facets are visible; the fibular facet appears slightly larger, although incomplete ossification of the distal femur makes this difficult to assess with confidence. Assorted limb elements are preserved near the femur and pelvic girdle, with another cluster further distally. The latter cluster is an articulated hind fin surrounded by preserved soft tissues (Figure 6D). As with *Stenopterygius* and *Hauffiopteryx*, the skeletal elements are situated asymmetrically within the soft tissue envelope, nearer to the leading edge of the fin than to the trailing edge (Maisch, 2008; Maxwell and Cortés, 2020). The tibia is large, with a convex proximal facet for articulation with the femur. The fibula appears to be missing or may be situated in the cluster of elements near the femur (Figure 6C). A large postaxial element is preserved, but is not associated with either proximal or distal elements. Functionally, the hind limb has three digits, the middle of which is the longest and the anterior of which is the shortest. Distally, the tibia articulates with a small distal tarsal (see Moon and Kirton, 2016), a large astragalus, and posteriorly with the fibula. The astragalus articulates entirely with the tibia, rather than being positioned between the tibia and fibula. The anterior digit has about three elements anterodistal to the tibia, the central digit has seven elements distal to the tibia, and the posterior digit has seven elements distal to the fibula. The distal posterior digit curves anteriorly, as in *Hauffiopteryx*. Although more rounded and less tightly articulated than the forelimb elements, the hind limb elements are less rounded and more tightly packed than those of *Ophthalmosaurus*.

Ontogeny. Numerous postcranial markers, including the orbit completely filled by the scleral ring (Fernández et al., 2005), open sutures between the forelimb elements (Johnson, 1977), lack of definition of the di- and parapophyses in the anterodorsal centra (Maxwell et al., 2016), and a broad neural canal are all indicative of the immature ontogenetic status of SNSB-BSPG 1954 I 608. Based on the number and unambiguous nature of these markers, in combination with the small size

of the individual, a relatively early postnatal stage can be inferred. Poor development of the capitulum and tuberculum is here tentatively suggested to represent a useful ontogenetic marker in ophthalmosaurians.

At 473 mm jaw length, SMNS 54067 is the largest specimen in the sample. Using the proportions of JME-SOS-08369, SMNS 54067 would correspond to an individual 1.98 m in total length (vs. 1.84 m for JME-SOS-08369). This is only 68% of the hypothetical maximum inferred length for this species (2.91 m); however, this maximum estimate assumes that SNSB-BSPG 1954 I 608 is a neonate and thus is likely an overestimate. Neither JME-SOS-08369 nor SMNS 54067 are well-enough preserved to confidently assess skeletal maturity. In any case, *Jabalisaurus tethyensis* was likely not a very large ichthyosaur species.

Soft tissue preservation. Despite originating from different formations and horizons and having undergone highly variable degrees of decay, all three specimens discussed here show extensive soft tissue preservation. In SNSB-BSPG 1954 I 608, this includes the outline of the hind fin (damaged post-collection, but still visible distally), as well as poorly preserved phosphatic remains concentrated mostly in the posterior abdominal region.

In JME-SOS-08369, the body outline is complete and has been described in detail elsewhere (Delsett et al., 2022). In the anterior dorsal region, a small accumulation of indeterminate ganoid scales are preserved, interpreted here as gut contents.

Lastly, in SMNS 54067, there are two types of soft tissue preservation, one of which is only clearly visible under UV-light. The soft tissue easily visible under natural light is located in the anterior abdominal region and dorsal to the vertebral column. Under natural light, the tissue has a cream-white colour and irregular folds, with fine regular ridges faintly visible beneath (Figure 8A). This soft tissue appears dark reddish-brown under UV-light (Figure 8B, D). The soft tissue that is only clearly visible under UV light appears yellow-orange (depending on the UV-light combination that is used) and is located anterodorsal to the other tissue type (Figure 8B–C). Using macro photography, very fine regular ridges are visible, running approximately parallel to the long axis of the body. The soft tissues preserved in this specimen are interpreted as the epidermis and dermis. The whitish, smooth tissue visible under natural light resembles the outermost layer of skin, with the smooth texture and irregular pattern resulting from decomposition forming folds (Lindgren et al., 2018). The second type is interpreted as the dermis, with the ridges corresponding either to dermal ridges formed at the epidermal-dermal interface (Lindgren et al., 2018) or dermal fibres (Lingham-Soliar, 2001). Regardless of interpretation, these morphologies correspond almost exactly with the skin of the early-diverging baracromian ichthyosaur *Stenopterygius* (Keller, 1992; Lindgren et al., 2018).

OPHTHALMOSAURIA indet.

Referred materials. NHMUK PV OR 42833 (Figure 11). A brief updated description is presented in Appendix 1.

Remarks. Meyer (1863) estimated that 45 mm was missing from the anterior rostrum of NHMUK PV OR 42833; here we consider this a substantial overestimate. Although the anteriormost premaxilla is damaged in this specimen, no more than a few millimeters is missing. The premaxilla contributes 51% to the dorsal snout, more consistent with *Jabalisaurus tethyensis* than *Aegirosaurus leptospondylus*, and the premaxillary and prenarial ratios are likewise more consistent with *J. tethyensis*. However, NHMUK PV OR 42833 cannot be referred to *Jabalisaurus tethyensis*: the rostrum does not appear to have been demarcated from the skull, as noted by Bardet and Fernández (2000), the prefrontal does not participate in the external narial opening, and the best-preserved tooth indicates that that the enamel was more coarsely ridged (Figure 11B), at ~8 ridges/5 mm. Given the lack of any named ichthyosaurian material from the German plattenkalk deposits exhibiting a similar character state combination, we do not consider this specimen to be referable to any genus at the present time; however, it unquestionably represents a third taxon, distinct from both *Aegirosaurus* and *Jabalisaurus*.

Results: Phylogenetic Analysis

Analysis under equal weights parsimony resulted in 80 MPTs of length 604, with most taxa within Ophthalmosauria resolved in a large polytomy. IterPCR pruned 10 taxa, including *Jabalisaurus meztli*, and resulted in the recovery of a sister-group relationship between *Ophthalmosaurus icenicus* and *J. tethyensis* at the base of Ophthalmosauria, whereas *Aegirosaurus* was resolved near the base of the platypterygiine subclade comprising *Caypullisaurus* and *Platypterygius*. Implied weights parsimony (k=12) resulted in a single MPT of length 26.72; *Jabalisarus meztli* and *J. tethyensis* formed a sister-group relationship within

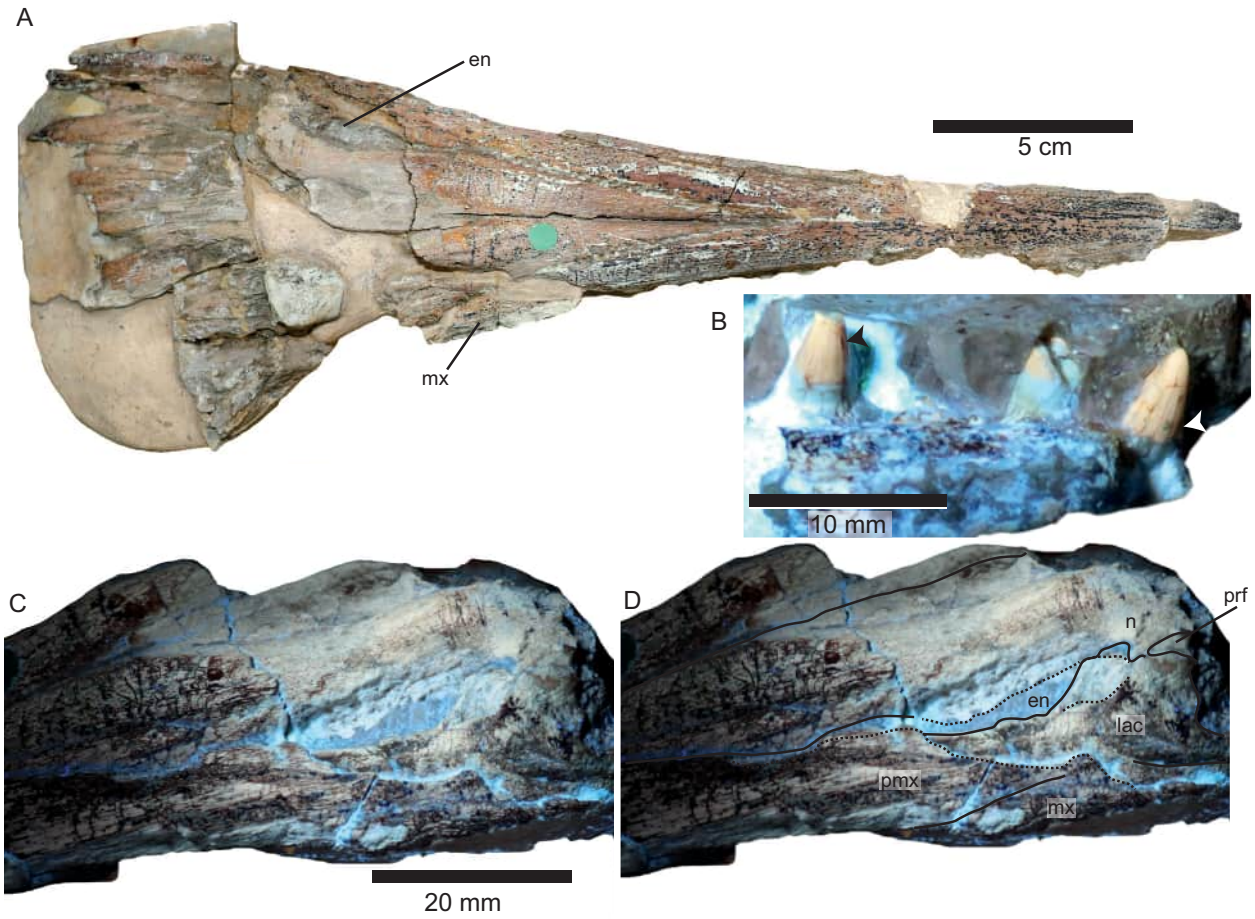

FIGURE 11. NHMUK PV OR 42833, Ophthalmosauria indet. A, anterior skull in dorsal view; B, maxillary dentition photographed under UV light. Black arrowhead indicates the fully erupted functional tooth showing weak to no development of apicobasal enamel ridges; white arrowhead indicates an erupting replacement tooth showing well-developed, widely spaced apicobasal enamel ridges. C, narial region photographed under UV-light; D, interpretation of narial region. Abbreviations: lac, lacrimal; en, external nares; mx, maxilla; n, nasal; pmx, premaxilla; prf, prefrontal. © The Trustees of the Natural History Museum, London.

Ophthalmosaurinae, whereas *Aegirosaurus* was sister to *Parrasaurus* in a resolved clade at the base of the platypterygiine subclade recovered under equal weights (Figure 12). Implied weights (k=9) resulted in five MPTs of length 32.60. *Jabalisaurus* spp. are optimized as the earliest-diverging ophthalmosaurians, whereas the ophthalmosaurines are distributed in a pectinate arrangement along the platypterygiine stem, rootward of *Aegirosaurus*. Implied weights (k=6) resulted in an incomplete search. Based on congruence with morphology, broad consistency with previously published topologies (Barrientos-Lara and Alvarado-Ortega, 2021b; Campos et al., 2025), and improved resolution relative to the equal weights tree, the IW k=12 topology is preferred.

DISCUSSION

Comparison to the Neotype of *Aegirosaurus leptospondylus*

Despite its early ontogenetic status, SNSB-BSPG 1954 I 608 is clearly distinct from the neotype of *Aegirosaurus leptospondylus*, including but not limited to having a less elongated snout (snout ratio of 0.62 vs. 0.73), of which the nasals form a proportionately greater contribution, a shorter, shallower maxilla (premaxillary ratio of 0.48 vs. 0.55), a larger eye, both in absolute as well as relative terms (orbital ratio of 0.26 vs. 0.18), a higher-crowned skull, a narial process of the prefrontal, bilobate external nares, absence of a humerus-intermedium contact and presence of a large facet for the preaxial element, and a much shorter and more rounded hind fin in which the tibia supports

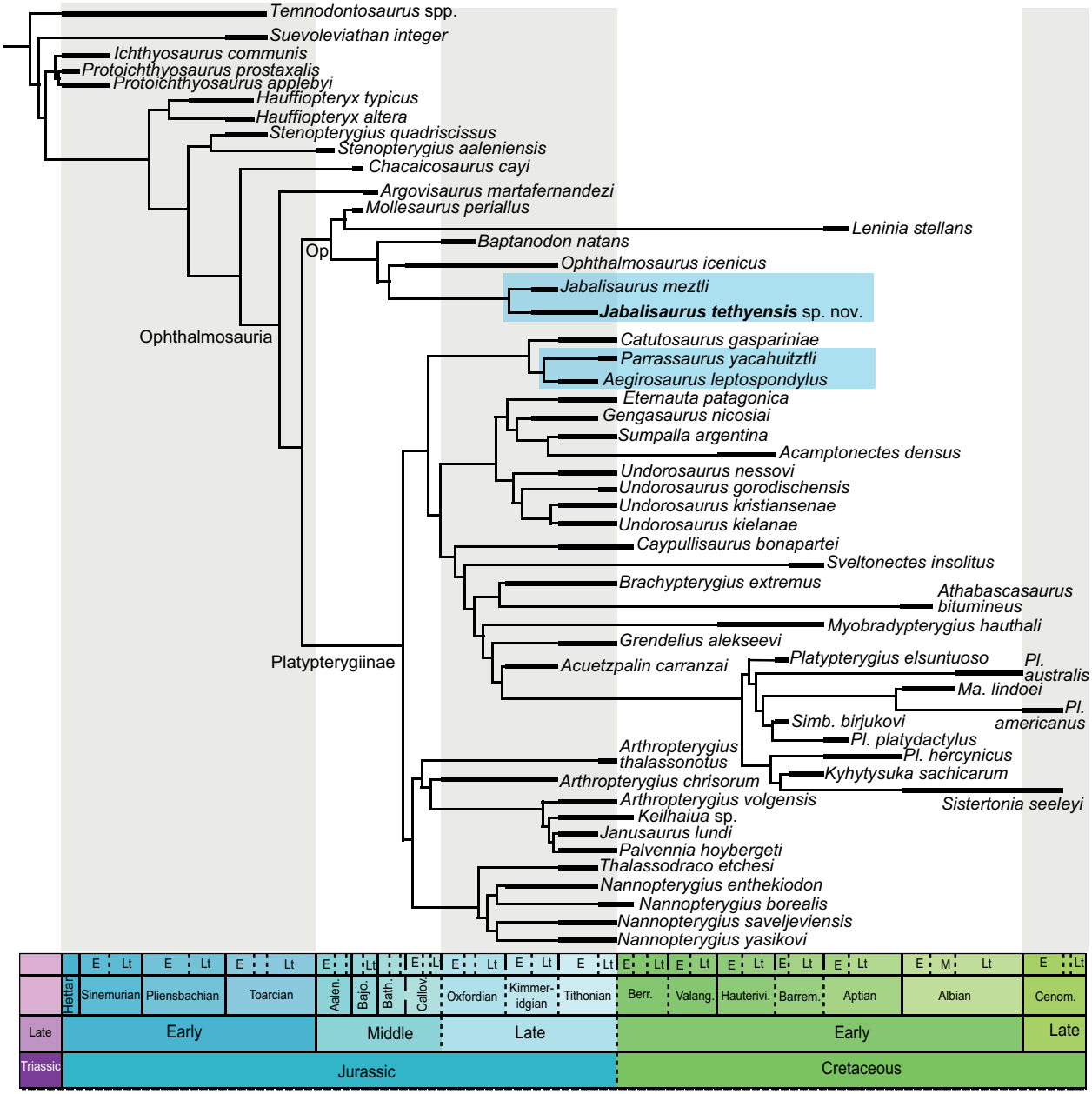

FIGURE 12. Phylogenetic analysis. Preferred topology (implied weights parsimony, k=12), single most parsimonious tree. No nodes within Ophthalmosauria received bootstrap support values >50%. Species pairs shared between the Late Jurassic of Germany and Mexico are highlighted in blue. Abbreviations: Op, Ophthalmosaurinae.

the astragalus to the exclusion of the fibula. While not all characters are visible on SMNS 54067 and JME-SOS-08369, the cranial ratio characters in these specimens (Table 1), as well as dental characters, differ from the *Aegirosaurus leptospondylus* neotype.

Comparison to *Jabalisaurus Meztli*

Jabalisaurus meztli is described as differing in a suite of characters from *J. tethyensis*, including the morphology of the posterodorsal narial region and the skull roof. Although we have not had the opportunity to personally examine the holotype material, photographs generously provided by MUDE can clarify a few of these characteristics. The posterolateral process of the frontal, contributing to its unique 'L'-shape, can confidently be identified as the anteromedial postfrontal, giving the skull roof a much more typical ophthalmosaurian configuration. The relationships between elements

in the narial region are difficult to understand, but it seems likely that the lacrimal-prefrontal suture is very similar in morphology to SMNS 54067, and that the anterior prefrontal is quite broad. However, as noted in the diagnosis of *Jabalisaurus tethyensis*, there is no indication that the splenial in this species plays as large a role in the lower jaw as in *J. meztli*. Moreover, *J. meztli* is of larger body size. Thus, we consider the two taxa to be distinct at the species level. The sister-group relationship between *J. meztli* and *J. tethyensis* to the exclusion of *Ophthlamosaurus icenicus* is supported by the presence of a descending process on the posterior dorsal border of the nares, a descending process of the nasal on the dorsal border of the nares, a gracile postorbital ramus of the jugal, a short medial contact between the parietals, and the presence of tightly packed polygonal phalanges.

Comparison to Other Late Jurassic Ophthalmosaurian Ichthyosaurs

Jabalisaurus tethyensis differs substantially from the large-bodied platypterygiines *Brachypterygius, Undorosaurus,* and *Caypullisaurus*, which are characterized by robust jaws, a proportionally long postorbital segment, and a rostrum not clearly offset from the skull, in addition to differences involving more subtle osteological features. *Caypullisaurus* and *Brachypterygius* are also characterized by substantial differences in forelimb construction: in *Caypullisaurus*, the intermedium is situated distal to the radius, rather than between the radius and ulna (Fernández, 2001), whereas in *Brachypterygius*, the intermedium articulates directly with the humerus (Moon and Kirton, 2018).

The platypterygiines *Sumpalla argentina* and *Eternauta patagonica*, from the Eastern Pacific of Argentina, while having a slenderer rostrum and less robust dentition than the above taxa, differ from *Jabalisaurus tethyensis* in several characters. *Sumpalla*, previously referred to *Aegirosaurus* (Gasparini et al., 2015), is characterized by a long interparietal suture, a strongly anteriorly deflected preaxial facet on the distal humerus, and the absence of medial fusion between the pubis and ischium in the pelvic girdle (Campos et al., 2021a). In contrast, *Eternauta patagonica* is more incomplete, but differs from *J. tethyensis* in the much more anteriorly extensive postorbital, slightly broader quadratojugal, absence of the squamosal, and the dentition, which has an enamel ridge density of only 5-6/5 mm (Campos et al., 2026; measured from fig. 8).

Jabalisaurus is quite similar to *Catutosaurus gaspariniae* from Argentina (Fernández et al., 2021); this genus also includes material formerly referred to *Aegirosaurus* (Maisch and Matzke, 2000). *C. gaspariniae i*s characterized by four articular facets on the distal humerus (vs. 3: *Jabalisaurus*), and the anterior facet is proportionately small. Moreover, the nasal dorsal to the external nares bears a long descending spur in *Catutosaurus*, rather than a broad constriction, and the tooth enamel is subtly ridged to smooth (Fernández et al., 2021). The participation of the splenial in the mandibular symphysis in *Catutosaurus* is extensive, more similar to *J. meztli* than to *J. tethyensis*.

In addition to rounded, loosely packed phalanges, *Arthropterygius* spp. differ from *J. tethyensis* in a broad posterolateral process of the parietal, and the absence of an obturator foramen in the ischiopubis (Delsett et al., 2017; Zverkov and Prilepskaya, 2019).

Gengasaurus, from coeval strata in Italy, is quite fragmentary, but differs from *J. tethyensis* in the relatively long, narrow humerus, with a small preaxial facet. The pentagonal radius of *J. tethyensis* also differs from the more rectangular radius (sensu Zverkov and Efimov, 2019) of *Gengasaurus*.

Jabalisaurus tethyensis bears a great resemblance to *Ophthalmosaurus icenicus* in overall cranial morphology, and also in postcranial morphology. *Jabalisaurus* spp. share a sister group relationship with *Ophthalmosaurus* based on a small, spur-like descending process of the nasal on the dorsal border of the nares and an interclavicle with a median stem equal or exceeding the length of the transverse bar. However, some notable differences are present between the taxa. The posterolateral process of the parietal is more elongate and slender in *J. tethyensis*, the anterior jugal contacts the premaxilla, the anterior process of the lacrimal does not extend as far anteriorly relative to the narial opening, and the narial process of the prefrontal is more prominent relative to *Ophthalmosaurus* (Moon and Kirton, 2016). These differences are more similar to the morphologies observed in *Nannopterygius*; however, *Jabalisaurus* differs from the latter genus in having a broad, plate-like ischiopubis, relatively prominent preaxial humeral facet, lack of indication of posteriorly pointed coracoids, and details of the dentition (Zverkov and Jacobs, 2020). Moreover, the polygonal phalanges in *Jabalisaurus* do not closely match the state in either *Ophthalmosaurus, Baptanodon, Thalas-*

sodraco, or *Nannopterygius*, with the exception of *N. saveljeviensis* (Zverkov and Jacobs, 2020).

Palaeobiogeography

The palaeobiogeography of Late Jurassic ichthyosaurian genera has been comprehensively discussed in the literature, with a focus on inferring potential dispersal corridors (Barrientos-Lara and Alvarado-Ortega, 2021a; Campos et al., 2021b) or, in studies undertaken prior to the extensive taxonomic revisions of the past decade, assuming a global distribution of genera (McGowan, 1978; Gasparini and Fernández, 1997; Bardet et al., 2014; Zverkov and Efimov, 2019). Both approaches addressed the problem in a similar way, i.e., asking what ichthyosaur distribution can tell us about palaeogeography and marine habitat connectivity in the Late Jurassic. From these approaches, and from a general understanding of ophthalmosaurian anatomy and palaeogeography, habitat connectivity is expected to have been high.

Despite the apparent high Late Jurassic marine habitat connectivity, the Late Jurassic ichthyosaurian fauna from the proto-Gulf of Mexico has been interpreted as being highly endemic (Barrientos-Lara and Alvarado-Ortega, 2021a). With the description of *Jabalisaurus tethyensis*, two closely related species-pairs have now been recovered from the German Plattenkalk deposits and the Gulf of Mexico region, namely *Jabalisaurus meztli* and *J. tethyensis*, and *Parrassaurus yacahuitztli* and *Aegirosaurus leptospondylus* (Figure 12; see also Barrientos-Lara and Alvarado-Ortega, 2021b). These findings challenge the hypothesis of strong endemicity in the Proto-Caribbean, and suggest instead a similar warm-temperate to tropical ichthyosaurian fauna across the northwestern Tethys and proto-Caribbean, possibly showing regional species-level divergence.

Differing from the Tethyan fauna noted above, high latitude European Late Jurassic localities are dominated by *Arthropterygius* spp. sensu Zverkov and Prilepskaya, 2019 (Svalbard: *Arthropterygius [Palvennia] hoybergeti, Ar. [Janusaurus] lundi, Ar. [Kelhauia]* sp., *Undorosaurus kristiansenae* [Delsett et al., 2019; Druckenmiller et al., 2012; Roberts et al., 2014]). *Arthropterygius* is also present in the sub-Boreal Province, although much less abundant. *Undorosaurus, Nannopterygius,* and *Brachypterygius* are widespread in the sub-Boreal Province (UK: *Brachypterygius extremus, Nannopterygius enthekiodon,* and *Thalassodraco etchesi* [Jacobs and Martill, 2020; Moon and Kirton, 2018; Zverkov and Jacobs, 2020]; Volga District: *Arthropterygius* sp., *Undorosaurus gorodischensis, U. nessovi, Brachypterygius pseudoscythicus, B. alekseevi, Nannopterygius saveljeviensis, N. yasykovi* [Zverkov et al., 2015; Zverkov and Efimov, 2019; Zverkov and Prilepskaya, 2019; Zverkov and Jacobs, 2020]; Poland: *Undorosaurus kielanae* [Tyborowski, 2016]). Although like *Arthropterygius*, *Undorosaurus* is found in both Boreal and sub-Boreal localities, it is in contrast more prevalent in sub-Boreal localities than Boreal ones. The Argentinian (temperate Eastern Pacific) fauna overlaps with the European faunas only in the presence of *Arthropterygius* (Campos et al., 2020); all other reported genera are endemic (*Catutosaurus gaspariniae, Sumpalla argentina, Caypullisaurus bonapartei,* and *Eternauta patagonica* [Fernández, 2007; Fernández et al., 2021; Campos et al., 2021, 2026]).

To explain these distributions patterns, we hypothesize that climate may have exerted a profound influence on ichthyosaurian palaeobiogeography, either indirectly due to its effects on prey species distribution and abundance, or due to inherent genus-level physiological temperature tolerances or adaptations to specific habitats, as in extant toothed whales (Whitehead et al., 2008).

Palaeobiological Significance

Despite a rich fossil record, the palaeobiology of Late Jurassic ichthyosaurs is poorly documented and is generally extrapolated from stratigraphically older taxa. Details of body and caudal fin shape are only known from the *Aegirosaurus leptospondylus* neotype (Bardet and Fernández, 2000), two indeterminate isolated caudal fins from the Tithonian of Germany (Bauer, 1898; Delsett et al., 2022), and *Jabalisaurus tethyensis* (JME-SOS-08369; Delsett et al., 2022). Soft-tissue fore- and hind limb outlines are known only for the *Aegirosaurus leptospondylus* neotype, and now the hind limb outline of the *J. tethyensis* holotype (Figure 6D). Unlike overall body outlines, which do not seem to show marked disparity between taxa, considerable variation in hind fin shape appears to have persisted into the Late Jurassic in ophthalmosaurians, including short, blunt, rounded fins in *J. tethyensis* (Figure 13), and more elongate, pointed fins in *Aegirosaurus*. SMNS 54067 cannot provide details regarding overall body shape; however, the smooth skin preserved in the anterior dorsal region is consistent with what has been reported in other baracromian ichthyosaurs (e.g., *Stenopterygius*, ?*Muiscasaurus* sp.) (Lindgren et al., 2018; Marti-

FIGURE 13. Artistic reconstruction of *Jabalisaurus tethyensis,* depicted in the water column close to the surface while pursuing halecomorph fishes. Watercolors, artwork by G.S.

nez-Motta et al., 2026) and adds to the growing body of literature on ichthyosaur skin morphology.

Likewise, direct evidence of diet has previously only been documented in two Late Jurassic ichthyosaurian taxa: an individual from the Oxfordian likely referable to *Baptanodon natans* (cephalopod hooklets: Massare and Young, 2005; Massare et al., 2014), and a small immature specimen from the Kimmeridge Clay likely referable to *Brachypterygius* sp. (actinopterygian fish remains and cephalopod hooklets: Naish and Moon, 2020). Gastric contents preserved in JME-SOS-08369 indicate that the diet of *J. tethyensis* included small ganoid-scaled actinopterygian fishes (Figure 13), contributing to this rather sparse record.

CONCLUSIONS

We report a second named genus of ophthalmosaurian ichthyosaur from the late Kimmeridgian–early Tithonian of Bavaria, Germany, *Jabalisaurus*, previously only known from the Kimmeridgian of Mexico. This increases the documented generic diversity of Late Jurassic ichthyosaurs from southern Germany, a finding that is consistent with the high ichthyosaurian genus-level diversity in sympatry documented from coeval Lagerstätte in both the northern and southern hemispheres.

We refer the German material to a new species, *J. tethyensis*, based on the reduced splenial contribution to the mandibular symphysis relative to the type species *J. meztli*, as well as and uncertainties regarding the influence of taphonomy on described cranial morphology in *J. meztli. J. tethyensis* is distinct from the co-occurring genus *Aegirosaurus* based on a suite of discrete and ratio-based cranial and postcranial characters.

Preserved gut contents suggest *Jabalisaurus tethyensis* consumed small bony fishes as part of its diet; soft-tissue preservation indicates that the skin on the torso was smooth, as in all baracromians documented thus far.

The occurrence of the genus *Jabalisaurus* in the northwestern Tethys weakens the interpretation of the proto-Caribbean region as a hotspot of ichthyosaur endemism during the Late Jurassic, suggesting instead that a tropical Tethyan ichthyosaurian fauna was broadly distributed glob-

ally, distinct from the more temperate to polar faunas described from the UK, Svalbard, and Russia, and Argentina.

ACKNOWLEDGMENTS

Thanks to S. Cooper (SMNS) for assisting with photographic documentation of JME-SOS-08369; C. Ifrim (JME), O. Rauhut (SNSB-BSPG), and M. Jones (NHMUK) for collections access, and to J. Madrazo Fanti (MUDE) for providing photos of *Jabalisaurus meztli*. The Lauer Foundation for Paleontology, Science and Education is profoundly thanked for providing to GS the necessary equipment for the triple wavelength UV analysis. GS was founded by an Erasmus + traineeship 2022/2023 program during the study and analysis of SMNS 54067.

REFERENCES

Arratia, G., Schultze, H.-P., Tischlinger, H., and Viohl, G. eds. 2015. Solnhofen: ein Fenster in die Jurazeit, Vol. 2. Dr. Friedrich Pfeil, Munich.

Bardet, N. and Fernández, M.S. 2000. A new ichthyosaur from the Upper Jurassic lithographic limestones of Bavaria. Journal of Paleontology, 74:503-511. https://doi.org/10.1666/0022-3360(2000)074<0503:ANIFTU>2.0.CO;2

Bardet, N., Falconnet, J., Fischer, V., Houssaye, A., Jouve, S., Pereda Suberbiola, X., Pérez-García, A., Rage, J.-C., and Vincent, P. 2014. Mesozoic marine reptile palaeobiogeography in response to drifting plates. Gondwana Research, 26:869-887. https://doi.org/10.1016/j.gr.2014.05.005

Barrientos-Lara, J.I. and Alvarado-Ortega, J. 2021a. A new ophthalmosaurid (Ichthyosauria) from the Upper Kimmeridgian deposits of the La Casita Formation, near Gómez Farías, Coahuila, northern Mexico. Journal of South American Earth Sciences, 111:103499. https://doi.org/10.1016/j.jsames.2021.103499

Barrientos-Lara, J.I. and Alvarado-Ortega, J. 2021b. A new Tithonian ophthalmosaurid ichthyosaur from Coahuila in northeastern Mexico. Alcheringa: An Australasian Journal of Palaeontology, 45:203-216. https://doi.org/10.1080/03115518.2021.1922755

Barthel, K.W. 1978. Solnhofen: ein Blick in die Erdgeschichte. Ott, Thun, Switzerland.

Barthel, K.W., Swinburne, N.H.M., and Morris, S.C. 1990. Solnhofen: a Study in Mesozoic Palaeontology. Cambridge University Press, Cambridge, UK.

Bauer, F. 1898. Die Ichthyosaurier des oberen weissen Jura. Palaeontographica, 44:283-328.

Benson, R.B.J., Butler, R.J., Lindgren, J., and Smith, A.S. 2010. Mesozoic marine tetrapod diversity: mass extinctions and temporal heterogeneity in geological megabiases affecting vertebrates. Proceedings of the Royal Society B, 277:829-834. https://doi.org/10.1098/rspb.2009.1845

Blainville, H.M.D. 1835. Description de quelques espèces de reptiles de la Californie, précédé de l'analyse d'un système général d'erpétologie et d'amphibiologie. Nouvelles Annales du Muséum d'Histoire Naturelle, Paris, 4:233-296.

Campos, L., Fernández, M.S., and Herrera, Y. 2020. A new ichthyosaur from the Late Jurassic of northwest Patagonia (Argentina) and its significance for the evolution of the narial complex of the ophthalmosaurids. Zoological Journal of the Linnean Society, 188:180-201. https://doi.org/10.1093/zoolinnean/zlz095

Campos, L., Fernández, M.S., Herrera, Y., and Garrido, A. 2021a. Morphological disparity in the evolution of the ophthalmosaurid forefin: new clues from the Upper Jurassic of Argentina. Papers in Palaeontology, 7:1995-2020. https://doi.org/10.1002/spp2.1374

Campos, L., Fernández, M.S., Herrera, Y., Talevi, M., Concheyro, A., Gouiric-Cavalli, S., O'Gorman, J.P., Santillana, S.N., Acosta-Burlaille, L., Moly, J.J., and Reguero, M.A. 2021b. Bridging the southern gap: First definitive evidence of Late Jurassic ichthyosaurs from Antarctica and their dispersion routes. Journal of South American Earth Sciences, 109:103259. https://doi.org/10.1016/j.jsames.2021.103259

Campos, L., Fernández, M.S., Herrera, Y., and Talevi, M. 2026. *Eternauta patagonica* gen. et sp. nov.: a new ophthalmosaurid ichthyosaur from the Upper Jurassic of Patagonia and its palaeoecological implications. Historical Biology, 38:1922-1945. https://doi.org/10.1080/08912963.2025.2568707

Cecca, F. 1999. Palaeobiogeography of Tethyan ammonites during the Tithonian (latest Jurassic). Palaeogeography, Palaeoclimatology, Palaeoecology, 147(1-2):1-37. https://doi.org/10.1016/S0031-0182(98)00149-7

Cleary, T.J., Moon, B.C., Dunhill, A.M., and Benton, M.J. 2015. The fossil record of ichthyosaurs, completeness metrics and sampling biases. Palaeontology, 58:521-536. https://doi.org/10.1111/pala.12158

Delsett, L.L., Roberts, A.J., Druckenmiller, P.S., and Hurum, J.H. 2017. A new ophthalmosaurid (Ichthyosauria) from Svalbard, Norway, and the evolution of the ichthyopterygian pelvic girdle. PLoS ONE, 12:e0169971. https://doi.org/10.1371/journal.pone.0169971

Delsett, L.L., Roberts, A.J., Druckenmiller, P.S., and Hurum, J.H. 2019. Osteology and phylogeny of Late Jurassic ichthyosaurs from the Slottsmøya Member Lagerstätte (Spitsbergen, Svalbard). Acta Palaeontologica Polonica, 64:717-743. https://doi.org/10.4202/app.00571.2018

Delsett, L.L., Friis, H., Köbl-Ebert, M., and Hurum, J.H. 2022. The soft tissue and skeletal anatomy of two Late Jurassic ichthyosaur specimens from the Solnhofen archipelago. PeerJ, 10:e13173. https://doi.org/10.7717/peerj.13173

Druckenmiller, P.S., Hurum, J.H., Knutsen, E.M., and Nakrem, H.A. 2012. Two new ophthalmosaurids (Reptilia: Ichthyosauria) from the Agardhfjellet Formation (Upper Jurassic: Volgian/Tithonian), Svalbard, Norway. Norwegian Journal of Geology, 92:311-339.

Fernández, M.S. 2001. Dorsal or ventral? Homologies of the forefin of *Caypullisaurus* (Ichthyosauria: Ophthalmosauria). Journal of Vertebrate Paleontology 21:515-520. https://doi.org/10.1671/0272-4634(2001)021[0515:dovhot]2.0.co;2

Fernández, M.S. 2007. Redescription and phylogenetic position of *Caypullisaurus* (Ichthyosauria: Ophthalmosauridae). Journal of Paleontology 81:368-375. https://doi.org/10.1666/0022-3360(2007)81[368:rappoc]2.0.co;2

Fernández, M.S. and Campos, L. 2015. Ophthalmosaurids (Ichthyosauria: Thunnosauria): alpha taxonomy, clades and names; pp. 20-30, In Fernández, M.S. and Herrera, Y. (eds.), Reptiles Extintos -Volumen en Homenaje a Zulma Gasparini. Publicación Electrónica de la Asociación Paleontológica Argentina. https://doi.org/10.5710/peapa.15.09.2015.96

Fernández, M.S., Archuby, F., Talevi, M., and Ebner, R. 2005. Ichthyosaurian eyes: paleobiological information content in the sclerotic ring of *Caypullisaurus* (Ichthyosauria, Ophthalmosauria). Journal of Vertebrate Paleontology, 25:330-337. https://doi.org/10.1671/0272-4634(2005)025[0330:IEPICI]2.0.CO;2

Fernández, M.S., Campos, L., Maxwell, E.E., and Garrido, A.C. 2021. *Catutosaurus gaspariniae*, gen. et sp. nov. (Ichthyosauria, Thunnosauria) of the Upper Jurassic of Patagonia and the evolution of the ophthalmosaurids. Journal of Vertebrate Paleontology, 41:e1922427. https://doi.org/10.1080/02724634.2021.1922427

Fischer, V., Clément, A., Guiomar, M., and Godefroit, P. 2011. The first definite record of a Valanginian ichthyosaur and its implications on the evolution of post-Liassic Ichthyosauria. Cretaceous Research, 32:155-163. https://doi.org/10.1016/j.cretres.2010.11.005

Fischer, V., Maisch, M.W., Naish, D., Kosma, R., Liston, J., Joger, U., Krüger, F.J., Pardo Pérez, J., Tainsh, J., and Appleby, R.M. 2012. New ophthalmosaurid ichthyosaurs from the European Lower Cretaceous demonstrate extensive ichthyosaur survival across the Jurassic-Cretaceous boundary. PLoS ONE, 7:e29234. https://doi.org/10.1371/journal.pone.0029234

Fischer, V., Bardet, N., Guiomar, M., and Godefroit, P. 2014. High diversity in Cretaceous ichthyosaurs from Europe prior to their extinction. PLoS ONE, 9:e84709. https://doi.org/10.1371/journal.pone.0084709

Fischer, V., Weis, R., and Thuy, B. 2021. Refining the marine reptile turnover at the Early–Middle Jurassic transition. PeerJ, 9:e10647. https://doi.org/10.7717/peerj.10647

Flannery Sutherland, J.T., Moon, B.C., Stubbs, T.L., and Benton, M.J. 2019. Does exceptional preservation distort our view of disparity in the fossil record? Proceedings of the Royal Society B, 286:20190091. https://doi.org/10.1098/rspb.2019.0091

Fürsich, F.T., Mäuser, M., Schneider, S., and Werner, W. 2007. The Wattendorf Plattenkalk (Upper Kimmeridgian) – a new conservation lagerstätte from the northern Franconian Alb, southern Germany. Neues Jahrbuch für Geologie und Paläontologie Abhandlungen, 245:45-58. https://doi.org/10.1127/0077-7749/2007/0245-0045

Gasparini, Z. and Fernández, M.S. 1997. Tithonian marine reptiles of the Eastern Pacific; pp. 435-450 In J. M. Callaway, and E. L. Nicholls (eds.), Ancient Marine Reptiles. Academic Press, San Diego, CA. https://doi.org/10.1016/B978-012155210-7/50023-5

Gasparini, Z., Fernández, M.S., De La Fuente, M., Herrera, Y., Codorniú, L., and Garrido, A. 2015. Reptiles from lithographic limestones of the Los Catutos Member (middle–upper Tithonian), Neuquén Province, Argentina: an essay on its taxonomic composition and preservation in an environmental and geographic context. Ameghiniana, 52:1-28. https://doi.org/10.5710/amgh.14.08.2014.2738

Gilmore, C.W. 1905. Osteology of *Baptanodon* (Marsh). Memoirs of the Carnegie Museum, 2:77-129.

Goloboff, P.A. and Morales, M.E. 2023. TNT version 1.6, with a graphical interface for MacOS and Linux, including new routines in parallel. Cladistics, 39:144-153. https://doi.org/10.1111/cla.12524

Jacobs, M.L. and Martill, D.M. 2020. A new ophthalmosaurid ichthyosaur from the Upper Jurassic (Early Tithonian) Kimmeridge Clay of Dorset, UK, with implications for Late Jurassic ichthyosaur diversity. PLoS ONE, 15:e0241700. https://doi.org/10.1371/journal.pone.0241700

Johnson, M.M., Mujal, E., Cooper, S.L.A., and Maxwell, E.E. 2025. Criteria for inferring seafloor arrival position in teleosauroid carcasses (Crocodylomorpha: Thalattosuchia) and comparison with other marine vertebrates. Geological Magazine, 162:1-18. https://doi.org/10.1017/S0016756825100058

Johnson, R. 1977. Size independent criteria for estimating relative age and the relationship among growth parameters in a group of fossil reptiles (Reptilia: Ichthyosauria). Canadian Journal of Earth Sciences, 14:1916-1924.

Kear, B.P. 2005. Cranial morphology of *Platypterygius longmani* Wade, 1990 (Reptilia: Ichthyosauria) from the Lower Cretaceous of Australia. Zoological Journal of the Linnean Society, 145:583-622. https://doi.org/10.1111/j.1096-3642.2005.00199.x

Keller, T. 1992. "Weichteil-Erhaltung" bei großen Vertebraten (Ichthyosauriern) des Posidonienschiefers Holzmadens (Oberer Lias, Mesozoikum Süddeutschlands). Kaupia: Darmstädter Beiträge zur Naturgeschichte, 1:23-62.

Kolb, C. and Sander, P.M. 2009. Redescription of the ichthyosaur *Platypterygius hercynicus* (Kuhn 1946) from the Lower Cretaceous of Salzgitter (Lower Saxony, Germany). Palaeontographica Abteilung A: Paläozoologie-Stratigraphie, 288:151-192. https://doi.org/10.1127/pala/288/2009/151

Lindgren, J., Sjövall, P., Thiel, V., Yheng, W., Ito, S., Wakamatsu, K., Hauff, R., Kear, B.P., Engdahl, A., Alwmark, C., Eriksson, M.E., Jarenmark, M., Sachs, S., Ahlberg, P.E., Marone, F., Kuriyama, T., Gustafsson, O., Malmberg, P., Thomen, A., Rodríguez-Meizoso, I., Uvdal, P., Ojika, M., and Schweitzer, M.H. 2018. Soft-tissue evidence for homeothermy and crypsis in a Jurassic ichthyosaur. Nature, 564:359-365. https://doi.org/10.1038/s41586-018-0775-x

Lingham-Soliar, T. 2001. The ichthyosaur integument: skin fibers, a means for a strong, flexible and smooth skin. Lethaia, 34:287–302. https://doi.org/10.1111/j.1502-3931.2001.tb00058.x

Lomax, D.R., Massare, J.A., and Maxwell, E.E. 2025. A new long and narrow-snouted ichthyosaur illuminates a complex faunal turnover during an undersampled Early Jurassic (Pliensbachian) interval. Papers in Palaeontology, 11:e70038. https://doi.org/10.1002/spp2.70038

Lukeneder, A., Zverkov, N., Kaurin, C., and Blüml, V. 2022. First Early Cretaceous ichthyosaurs of Austria and the problem of Jurassic-Cretaceous ichthyosaurian faunal turnover. Cretaceous Research, 136:105224. https://doi.org/10.1016/j.cretres.2022.105224

Maisch, M.W. 2008. Revision der Gattung *Stenopterygius* Jaekel, 1904 emend. von Huene, 1922 (Reptilia: Ichthyosauria) aus dem unteren Jura Westeuropas. Paleodiversity, 1:227-271.

Maisch, M.W. 2015. Fischechsen (Ichthyosauria); pp. 422-430, In Arratia, G., Schultze, H.-P., Tischlinger, H., and Viohl, G. (eds.), Solnhofen: ein Fenster in die Jurazeit. Dr. Friedrich Pfeil, Munich.

Maisch, M.W. and Matzke, A.T. 2000. The Ichthyosauria. Stuttgarter Beiträge zur Naturkunde Serie B (Geologie und Paläontologie), 298:1-159.

Martinez-Motta, M.F., Cortés, D., Maxwell, E.E., Noè, L., Alfonso-Rojas, A., Parra-Ruge, F., and Cadena, E.-A. 2026. Soft-tissue preservation in an ichthyosaur from the Lower Cretaceous (Barremian - Aptian) of Colombia. Cretaceous Research, 181:106305. https://doi.org/10.1016/j.cretres.2025.106305

Massare, J.A. and Connely, M.V. 2022. Braincase morphology of *Baptanodon natans* (Reptilia: Ichthyosauria). Paludicola, 14:43-56.

Massare, J.A. and Young, H.A. 2005. Gastric contents of an ichthyosaur from the Sundance Formation (Jurassic) of Central Wyoming. Paludicola, 5:20-27.

Massare, J.A., Wahl, W.R., Ross, M., and Connely, M.V. 2014. Palaeoecology of the marine reptiles of the Redwater Shale Member of the Sundance Formation (Jurassic) of central Wyoming, USA. Geological Magazine, 151:167-182. https://doi.org/10.1017/S0016756813000472

Maxwell, E.E. 2012. Unraveling the influences of soft-tissue flipper development on skeletal variation using an extinct taxon. Journal of Experimental Zoology (Molecular and Developmental Evolution), 318:545-554. https://doi.org/10.1002/jez.b.22459

Maxwell, E.E. and Cortés, D. 2020. A revision of the Early Jurassic ichthyosaur *Hauffiopteryx* (Reptilia: Ichthyosauria), and description of a new species from southwestern Germany. Palaeontologia Electronica, 23:a31. https://doi.org/10.26879/937

Maxwell, E.E., Scheyer, T.M., and Fowler, D.A. 2014. An evolutionary and developmental perspective on the loss of regionalization in the limbs of derived ichthyosaurs. Geological Magazine, 151:29-40. https://doi.org/10.1017/S0016756812001070

Maxwell, E.E., Dick, D., Padilla, S., and Parra, M.L. 2016. A new ophthalmosaurid ichthyosaur from the Early Cretaceous of Colombia. Papers in Palaeontology, 2:59-70. https://doi.org/10.1002/spp2.1030

McGowan, C. 1976. The description and phenetic relationships of a new ichthyosaur genus from the Upper Jurassic of England. Canadian Journal of Earth Sciences, 13:668-683. https://doi.org/10.1139/e76-070

McGowan, C. 1978. Further evidence for the wide geographical distribution of ichthyosaur taxa (Reptilia: Ichthyosauria). Journal of Paleontology, 52:1155-1162.

McGowan, C. 1992. Unusual extensions of the neural spines in two ichthyosaurs from the Lower Jurassic of Holzmaden. Canadian Journal of Earth Sciences, 29:380-383. https://doi.org/10.1139/e92-034

McGowan, C. and Motani, R. 2003. Ichthyopterygia. Verlag Dr. Friedrich Pfeil, München.

Meyer, H. 1863. *Ichthyosaurus leptospondylus* Wag.? aus dem lithographischen Schiefer von Eichstätt. Palaeontographica, 11:222-225.

Miedema, F. and Maxwell, E.E. 2022. Ontogenetic variation in the skull of *Stenopterygius quadriscissus* with an emphasis on prenatal development. Scientific Reports, 12:1707. https://doi.org/10.1038/s41598-022-05540-0

Moon, B.C. and Kirton, A.M. 2016. Ichthyosaurs of the British Middle and Upper Jurassic. Part 1, *Ophthalmosaurus*. Palaeontographical Society, London. https://doi.org/10.1080/02693445.2016.11963958

Moon, B.C. and Kirton, A.M. 2018. Ichthyosaurs of the British Middle and Upper Jurassic. Part 2, *Brachypterygius, Nannopterygius, Macropterygius* and taxa invalida. Palaeontographical Society, London. https://doi.org/10.1080/02693445.2018.1468139

Moon, B.C. and Stubbs, T.L. 2020. Early high rates and disparity in the evolution of ichthyosaurs. Communications Biology, 3:68. https://doi.org/10.1038/s42003-020-0779-6

Motani, R. 1999a. On the evolution and homologies of ichthyopterygian forefins. Journal of Vertebrate Paleontology, 19:28-41. https://doi.org/10.1080/02724634.1999.10011120

Motani, R. 1999b. Phylogeny of the Ichthyopterygia. Journal of Vertebrate Paleontology, 19:472-495. https://doi.org/10.1080/02724634.1999.10011160

Naish, D. and Moon, B. 2020. 4. Ichthyosaurs; pp. 75-90, In Martill, D.M. and Etches, S. (eds.), Fossils of the Kimmeridge Clay Formation. Volume 2. Palaeontological Association, London.

Niebuhr, B. and Pürner, T. 2014. Plattenkalk und Frankendolomit – Lithostratigraphie der Weißjura-Gruppe der Frankenalb (außeralpiner Oberjura, Bayern). Schriftenreihe der Deutschen Gesellschaft für Geowissenschaften, 83:5-72. https://doi.org/10.1127/sdgg/83/2014/5

Páramo-Fonseca, M.E., García Guerrero, J., Benavides-Cabra, C.D., Padilla Bernal, S., and Casteñeda-Gómez, A.J. 2021. A benchmark specimen of *Muiscasaurus catheti* from the upper Aptian of Villa de Leiva, Colombia: new anatomical features and phylogenetic implications. Cretaceous Research, 119:104685. https://doi.org/10.1016/j.cretres.2020.104685

Quenstedt, F.A. 1856-1858. Der Jura. H. Laupp, Tübingen.

Roberts, A.J., Druckenmiller, P.S., Saetre, G.-P., and Hurum, J.H. 2014. A new Upper Jurassic ophthalmosaurid ichthyosaur from the Slottsmøya Member, Agardhfjellet Formation of Central Spitsbergen. PLoS ONE, 9:e103152. https://doi.org/10.1371/journal.pone.0103152

Sander, P.M. 2000. Ichthyosauria: their diversity, distribution and phylogeny. Paläontologische Zeitschrift, 74:1-35. https://doi.org/10.1007/bf02987949

Scheyer, T.M. and Moser, M. 2011. Survival of the thinnest: rediscovery of Bauer's (1898) ichthyosaur tooth sections from the Upper Jurassic lithographic limestone quarries, south Germany. Swiss Journal of Geosciences, 104:147-157. https://doi.org/10.1007/s00015-011-0076-y

Schweigert, G. 2007. Ammonite biostratigraphy as a tool for dating Upper Jurassic lithographic limestones from South Germany – first results and open questions. Neues Jahrbuch für Geologie und Paläontologie Abhandlungen, 245:117-125. https://doi.org/10.1127/0077-7749/2007/0245-0117

Serafini, G., Maxwell, E.E., Fornaciari, E., and Papazzoni, C.A. 2022. Revision of platypterygiine rostral material from the Northern Apennines (Italy): new insights on distal neurovascular anatomy and tooth replacement in Cretaceous ichthyosaurs. Cretaceous Research, 135:105167. https://doi.org/10.1016/j.cretres.2022.105167

Tyborowski, D. 2016. A new ophthalmosaurid ichthyosaur from the Late Jurassic of Owadów-Brzezinki Quarry, Poland. Acta Palaeontologica Polonica, 61:791-803. https://doi.org/10.4202/app.00252.2016

Viohl, G. 2015a. Die Plattenkalk-Typen der Südlichen Frankenalb; pp. 72-77, In Arratia, G., Schultze, H.-P., Tischlinger, H., and Viohl, G.(eds.), Solnhofen: ein Fenster in die Jurazeit Dr. Friedrich Pfeil, München.

Viohl, G. 2015b. Der geologische Rahmen: die Südliche Frankenalb und ihre Entwicklung; pp. 56-62, In Arratia, G., Schultze, H.-P.,Tischlinger, H., and Viohl, G. (eds.), Solnhofen: ein Fenster in die Jurazeit. Dr. Friedrich Pfeil, München.

Wagner, A. 1852. Neu aufgefundene Saurier Ueberreste aus den lithographischen Schiefern und dem obern Jurakalke. Abhandlungen der Mathematischen-Physikalischen Classe der Königlich Bayerischen Akademie der Wissenschaften, 6:661-710.

Wagner, A. 1853a. Die Characteristik einer neuen Art von *Ichthyosaurus* aus den lithographischen Schiefern und eines Zahnes von *Polyptychodon* aus dem Grünsandsteine von Kelheim. Gelehrte Anzeigen der königlich bayerischen Akademie der Wissenschaften, 36:25-32.

Wagner, A. 1853b. Beschreibung einer fossilen Schildkröte und etlicher anderer Reptilien-Ueberreste aus den lithographischen Schiefern und dem Grünsandsteine von Kelheim. Abhandlungen der mathematisch-physikalischen Classe der königlich bayerischen Akademie der Wissenschaften, 7:239-264.

Wagner, A. 1861. Neue Beiträge zur Kenntniss der urweltlichen Fauna des lithographischen Schiefers. Abhandlungen der Mathematische-Physikalischen Classe der königlich bayerischen Akademie der Wissenschaften, 9:65-124.

Wahl, W.R. 2009. Taphonomy of a nose dive: bone and tooth displacement and mineral accretion in an ichthyosaur skull. Paludicola, 7:107-116.

Westermann, G.E. 2000. Marine faunal realms of the Mesozoic: review and revision under the new guidelines for biogeographic classification and nomenclature. Palaeogeography, Palaeoclimatology, Palaeoecology, 163(1-2):49-68. https://doi.org/10.1016/s0031-0182(00)00142-5

Whitehead, H., McGill, B., and Worm, B. 2008. Diversity of deep-water cetaceans in relation to temperature: implications for ocean warming. Ecology Letters, 11:1198-1207. https://doi.org/10.1111/j.1461-0248.2008.01234.x

Zverkov, N.G. and Efimov, V.M. 2019. Revision of *Undorosaurus*, a mysterious Late Jurassic ichthyosaur of the Boreal Realm. Journal of Systematic Palaeontology, 17:1183-1213. https://doi.org/10.1080/14772019.2018.1515793

Zverkov, N.G. and Jacobs, M.L. 2020. Revision of *Nannopterygius* (Ichthyosauria: Ophthalmosauridae): reappraisal of the 'inaccessible' holotype resolves a taxonomic tangle and reveals an obscure ophthalmosaurid lineage with a wide distribution. Zoological Journal of the Linnean Society, 191:228-275. https://doi.org/10.1093/zoolinnean/zlaa028

Zverkov, N.G. and Prilepskaya, N.E. 2019. A prevalence of *Arthropterygius* (Ichthyosauria: Ophthalmosauridae) in the Late Jurassic—earliest Cretaceous of the Boreal Realm. PeerJ, 7:e6799. https://doi.org/10.7717/peerj.6799

Zverkov, N.G., Arkhangelsky, M.S., and Stenshin, I.M. 2015. A review of Russian Upper Jurassic ichthyosaurs with an intermedium/humeral contact. Reassessing *Grendelius* McGowan, 1976. Proceedings of the Zoological Institute RAS, 319:558-588. https://doi.org/10.31610/trudyzin/2015.319.4.558

APPENDIX 1.

Brief description of *Aegirosaurus leptospondylus* based on the SNSB-BSPG cast

General observations. The skull is low-crowned, with an unusually long, slender snout (snout ratio = 0.73), an oval orbit, and a small eye relative to skull length (Fernández et al., 2005). The skull constitutes almost 50% of presacral length. As noted in the initial description, the forefin appears to be characterized by open sutures between elements. Both the proportionately large skull and characters indicative of osteological immaturity in the forefin support a juvenile interpretation for this specimen (Bardet and Fernández, 2000), but the small size of the scleral ring relative to the orbit as well as the orbit relative to the skull are more consistent with an adult (Fernández et al., 2005). The mid- to anteriormost rostrum suffered deformation, exhibiting both ventral bending and lateral torsion (roughly 30°) due to lithostatic compression. The tip of the upper jaw is fractured, resulting in a taphonomic underbite.

Premaxilla. The premaxilla is very elongate. Anteriorly, it is marked by a relatively prominent although discontinuous premaxillary fossa; this becomes very shallow and poorly defined towards the nares. The posterior premaxilla is relatively deep immediately anterior to the external nares (Figure 2A). Bardet and Fernández (2000) illustrate a supranarial process; while this is not entirely clear in the cast, the depth of the premaxilla anterior to the narial opening makes it seem likely. Dorsally, the premaxilla makes up 63% of the snout, with the nasals contributing the remaining 37% (Figure 2C).

Narial region. Sutures ventral to the narial opening are not visible in the cast. Relative to the external nares, the anterior process of the maxilla is rather elongate, but because the rostrum is so long, the maxilla only makes up a small percentage of the snout (22%). The deepest exposed point of the maxilla is ventral to the external naris. The area below the nares is relatively deep; thus the round narial opening is positioned close to the orbit and relatively high on the snout (Figure 2A, D). The posterodorsal corner of the naris is overhung by a small, laterally projecting flange. There is no space for an externally open anterior narial opening.

In contrast to the situation illustrated in Bardet and Fernández (2000: fig. 3), we consider the suture between the lacrimal and nasal to be near the dorsal edge of the nares. The lacrimal thus forms the entire posterior border of the nares, and contacts the nasal dorsally. The posterior edge of the lacrimal projects laterally in a ridge. Bardet and Fernández (2000): fig. 3 illustrate the lacrimal as contributing to a recessed circumorbital area. Based on the photo of the neotype, the lack of bone-like texture on this surface in the cast, the absence of a large anterior circumorbital area on the poorly preserved left side of the cast, and agreement in orbital length measurements, this surface seems likely to be sediment.

Nasal. The nasals have a very unusual morphology in the internarial region. Posterior to the V-shaped articulation with the premaxillae, they form a second V-shaped articulation (Figure 2C). Whether this is a very weak compaction fracture caused by the skull penetrating into the sediment or a lamina of bone extending anteriorly to close the internarial foramen requires additional material. The internasal depression is present, but not strongly developed. Our interpretation of the nasal-frontal suture is less deeply concave than that reconstructed by Bardet and Fernández (2000), with greater overlap of the postfrontal (Figure 2C).

Frontal. As reconstructed by Bardet and Fernández (2000), the frontals have substantial exposure on the dorsal skull roof, and form the anterior edges of the upper temporal fenestra (UTF) (Figure 2C, E). The parietal foramen is located on the frontal-parietal suture, but is more enclosed by the frontals than the parietals, which only contribute to the posterior margin in dorsal view. The anterior frontals form two ridges oriented roughly anteroposteriorly from the nasal frontal-suture that reach a high point on the anterior margin of the parietal foramen. Lateral to this ridge, there is a depression on the anteromedial corner of the UTF, and medial to the ridge is a prominent interfrontal depression anterior to the parietal foramen. A weak convexity separates most of the anterior UTF from a weakly developed anterior terrace formed by the frontal and posterior nasal. The frontal appears to contact the supratemporal on the anterolateral internal edge of the UTF, thus excluding the postfrontal.

Parietal. The interparietal suture is relatively elongated. The parietals are medially raised, but do not form a defined ridge along the suture. Anteriorly, the parietals broadly diverge, enclosing the frontals and forming the entire medial edge of the UTF. Posteriorly, development of the postparietal ridge is difficult to assess in the cast – while a roughened area for muscle attachment is present (as in e.g., *Platypterygius australis*), this does not appear to form a depressed posterior lamina enclosing the supraoccipital. The supratemporal-parietal contact cannot be assessed with confidence in the cast.

Supratemporal. In dorsal view, the supratemporal encloses the posterior and lateral edges of the UTF, and appears to send a short internal process medially to contact the frontal (Figure 2C, E). Laterally, the situation is not clear in the cast.

Cheek region. The cheek region is very difficult to interpret in the cast (Figure 2A). On the right side of the skull, the quadratojugal might be missing, resulting in a concave posterior cheek and leaving parts of the quadrate laterally exposed. A small fragment of the quadratojugal may be present ventrally, but does not appear to be complete dorsally. Likewise, the squamosal appears to be fragmentary. The postorbital is as illustrated by Bardet and Fernández (2000), overlapping the jugal ventrally.

Jugal. The jugal is L-shaped, with a relatively straight ventral ramus and a small posterior heel. Anteriorly, its sutural contacts cannot be determined in the cast (Figure 2A, D). The jugal has an extremely distinctive morphology of the ventral ramus, being mediolaterally broad and flat, and dorsoventrally narrow, forming a sharp ridge along its lateral surface ventral to the orbit.

Lower jaw. The lower jaw is straight ventral to the orbit, and appears to have a lateral orientation rather than curving posteromedially. The extent of the angular, surangular, and dentary are as illustrated by Bardet and Fernández (2000), although it should be noted that the greater anterior extent of the surangular than the angular is potentially caused by incomplete preparation, as the complete lateral surface of the mandible is not exposed in this region. The lateral surangular is very distinctive: the surangular fossa is extremely short and shallow, almost non-existent. The lateral surface of the surangular is pierced by two foramina, a smaller posterior one and the larger one continuous with the main part of the fossa, very similar to the state illustrated in the holotype of '*I.' leptospondylus* (Bauer, 1898).

Dentition. The teeth are relatively slender, and are strongly ornamented with enamel ridges (Figure 2B). The ridges are less densely packed than in *Jabalisaurus tethyensis* sp. nov. (8-10/5 mm vs. 17-18/5 mm: Serafini et al., 2022), and appear to extend from the base of the enamel to the tooth apex. The base of the enamel is very well defined, clearly visible even in the cast. Basal to the enamel, the surface of the tooth root is smooth, presumably consisting of acellular cementum.

Ophthalmosauria indet.

Referred material. NHMUK PV OR 42833 (Figure 11).

General observations. The preserved length of the specimen is 312 mm, with a snout length of 250 mm. While a few millimeters may be missing from the anterior right-hand premaxilla, the snout appears almost complete on the better-preserved left side (Figure 11A). The skull appears poorly mineralized, with abundant vascularization and evidence of plastic deformation of thin bony laminae, suggesting that this specimen represents an ontogenetically very young individual. As noted by Bardet and Fernández (2000), the snout appears to be poorly demarcated from the posterior skull.

The posteriormost preserved part of the skull consists of a series of thin bones/laminae running parallel to the long axis of the rostrum. These likely represent elements of the palate and/or mandible, damaged to varying degrees; individual bones cannot be identified.

Premaxilla. The premaxillary fossa is present as a series of foramina anteriorly, and a weakly developed groove posteriorly. The premaxillae contribute 51% to the dorsal surface of the snout (127 mm). In dorsal view, the anterior part of the premaxilla-nasal contact is complex, with the pre-

maxilla forming a series of thin bony protrusions that created a more robust contact with the underlying nasal rather than a simple overlapping suture. Posteriorly, the subnarial process of the premaxilla extends the entire length of the narial opening, overlapping the maxilla ventrally and articulating with the lacrimal posterodorsally and possibly the jugal posteriorly.

Maxilla. The maxilla has relatively limited lateral exposure, both in general and anterior to the external nares, comprising approximately 1/3 of the antorbital rostrum. It is excluded from the narial opening by the surrounding bones, and lacks a narial process (Figure 11C–D). A groove on the posterolateral maxilla, ventral to the lacrimal, likely represents the articular facet for the jugal.

Nasal. The anterior nasals are well preserved, but posterior to the external nares these are broken. Anterodorsal to the external nares, the nasal is ornamented with parallel grooves and foramina. The nasal makes up the dorsal edge of the external narial opening. While the bony naris appears to be weakly bilobate, a prominent descending pillar of the nasal is absent (Figure 11C, D). Posterior to the nares, the nasal contacts the lacrimal anteroventrally and the prefrontal posteroventrally.

Lacrimal. The lacrimal forms the anterior edge of the orbit, and the ventral edge of the posterior external nares. A posterolateral ridge delimits the anterior circumorbital area. The lacrimal is relatively broad and robust, increasing the distance between the orbit and the external nares. Dorsally, the lacrimal contacts the nasal anteriorly, and the prefrontal posteriorly (Figure 11C–D).

Prefrontal. Only the anteroventralmost prefrontal is preserved, posterodorsal to the external nares (Figure 11C–D). Participation in the external nares by the prefrontal was clearly absent.

Dentition. The teeth are well-preserved, especially posteriorly. As noted by Meyer (1863), the teeth show a mixture of smooth and coarsely ridged enamel, with the smaller functional teeth showing almost smooth enamel, whereas the larger replacement teeth show clear ridging (Figure 11B). The enamel ridges do not extend to the crown apex, and are quite coarsely spaced, with a density of ~8 ridges/5 mm despite the minute size of the teeth.

APPENDIX 2.

Phylogenetic analysis

Scoring modifications

Baptanodon natans: Ch. 46-49, 51, 53, 57, and 63 were scored for the first time based on Massare and Connely (2022).

Jabalisaurus meztli: Ch. 9, 29 were rescored based on photos of the holotype specimen.

Character List

From Campos et al. (2025); characters 9 and 15 have been modified from their formulation in the original work.

1- Crown striations: presence of deep axial ridges (0), crown enamel subtly ridged or smooth (1). (Druckenmiller and Maxwell 2010, character 25).

2- Base of enamel layer on crown: weakly defined, invisible (0), well defined, precise (1). (Fischer et al., 2011, character 2).

3- Root cross-section in mid-jaw teeth of adults: rounded (0), quadrangular (1). (Fischer et al., 2011, character 3).

4- Plicidentine: Vertical grooves present basal to the crown and apical to the root osteocementum (0); this region of the tooth appears smooth (1). (Maxwell et al., 2016, character 4).

5- Deep apicobasal grooves in root: present (0), absent (1). (Fischer et al., 2016, character 4).

6- Processus postpalatinis pterygoidei: absent (0), present (1). (Maisch and Matzke 2000, character 38).

7- Forked posterior process on the pterygoid: absent (0), present (1) (Campos et al., 2020, character 69).

8- Pterygoid lamellae proportions: lateral lamella more developed in mediolateral direction than the medial lamella (0), medial lamella more developed in mediolateral direction than the lateral lamella (1). (Campos 2022, character 9).

9- Maxilla, lateral view: (0) premaxillary process long, extending approximately 1.5 narial lengths or more anterior to external nares; premaxillary process short, extending approximately 1 narial lengths or less anterior to external narial opening (1) (Maxwell et al., 2012, character 2, modified from Fernandez 2007, character 1).

10- Postnarial process of the maxilla in lateral view: present (0), absent (1). (Maxwell and Cortés 2020, character 11, modified from Maisch and Matzke 2000, character 11).

11- Size of the jugal process of the maxilla: short, hidden from lateral view by jugal (0), long, extending as far under orbit as lacrimal in lateral view; (1). (Maxwell et al., 2012, character 3) (inverted coding).

12- Dorsal exposure of the nasal: (0) substantial, dorsally exposed over more than 40% or more of the prenarial rostrum (0), reduced, dorsally exposed over less than 40% prenarial rostral length (1). (Maxwell et al., 2012, character 4).

13- Descending process of the nasal on the posterior dorsal border of the nares: absent (0), present (1). (Fernández 2007, character 2).

14- Descending process of the nasal on the dorsal border of the nares: absent (0), spur-like and short (1), spur-like and long, almost dividing completely the naris (2), stout descending process of the nasal forming a pillar with the ascending process of the maxilla (3). (Campos et al., 2020, character 7).

15- Complete division of the external naris: present, with equal contributions of the maxilla and the nasal (0), present, predominantly by means of the ascending process of the maxilla that reaches the ventral portion of the nasal (1). (Campos 2022, character 16).

16- Premaxilla/lacrimal contact below the external naris: present and preventing the maxilla from reaching the external naris (0); present, although the maxilla reaches the external naris (1); absent (2). (Campos 2022, character 17, modified from Fernández 2007, character 0).

17- Processus supranarialis of the premaxilla: present (0), absent (1). (Maisch and Matzke 2000, character 10).

18- Processus subanarialis of the premaxilla: ends anteriorly to posterior end of the external naris (0), reaches posterior end of the external naris (1), absent (2). (Modified from Fischer et al., 2016, character 7)

19- Lacrimal contribution to the external naris: present (0), absent, the lacrimal is excluded from the border of the external naris by the nasal and/or the maxilla (1). (Sander 2000, character 10).

20- Processus narialis of the prefrontal: absent (0), present (1). (Fischer et al., 2011, character 11).

21- Anterior margin of jugal I: tapering, running between the lacrimal and maxilla (0), broad and fan-like, covering large area of maxilla ventrolaterally (1). (Duckenmiller and Maxwell 2010, character 6).

22- Anterior margin of the jugal: terminates prior to anterior end of lacrimal (0), reaches or surpasses anterior end of lacrimal (1). (Roberts et al., 2014, character 11).

23- Posterior margin of the jugal: articulates with the postorbital and quadratojugal (0); excluded from the quadratojugal by the postorbital (1). (Roberts et al., 2014, character 12).

24- Postorbital portion of the jugal: gracile (0), anteroposteriorly wide (1). (Zverkov and Efimov 2019, character 23).

25- Jugal/premaxilla contact: absent (0), present (1). (Zverkov and Efimov 2019, character 21).

26- Postorbital contribution to the ventral border of the orbit: absent (0); discreet, the anterior extension of the ventral contribution of the postorbital does not reach the anterior half of the orbit (1); large, the ventral contribution of the postorbital reaches the anterior half of the orbit (2). (Campos 2022, character 27).

27- Supratemporal processes of the parietals: relatively thin, the width of the process is equal to or less than 0.5 of the width of the main body of the parietal (0); robust, the width of the processes is greater than 0.5 of the width of the main body of the parietals (1). (Modified from Zverkov and Efimov 2019, character 31).

28- Sagittal eminence: present (0), absent (1). (Fernández 2007, character 5 modified from Motani 1999, character 16).

29- Medial contact between the parietals: anteroposteriorly long, the contact extends beyond half of the anteroposterior length of the main body of the parietals (0), anteroposteriorly short, the contact does not extend beyond half of the anteroposterior length of the main body of the parietals (1). (Modified from Zverkov and Prilepskaya 2019, character 108).

30- Location of the parietal foramen: completely surrounded by the parietals (0), on the fronto-parietal suture (1), entirely surrounded by the frontals (2). (Modified from Motani 1999, character 19).

31- Processus temporalis of the frontal: absent (0); present (1). (Fischer et al., 2011, character 14).

32- Contact between nasal and postfrontal: Present (0), absent (1). (Campos 2022, character 33).

33- Supratemporal-postorbital contact: absent (0), present (1). (Sander 2000, character 27) (Inverted coding).

34- Supratemporal–stapes contact: absent, the posteroventral process of the supratemporal does not extend up to the shaft of the stapes (0), present (1). (Fischer et al., 2016, character 26).

35- Anteromedial process of the supratemporal: absent or poorly developed, shorter than the anterolateral process (0); present and longer than the anterolateral process, not reaching the parietal (1); present and reaching the parietal (2). (Modified from Fischer et al., 2016, character 24).

36- Broad postfrontal-postorbital contact: absent (0), present (1). (Roberts et al., 2014, character 16).

37- Squamosal shape: triangular (0), squared (1), squamosal absent (2). (Fischer et al., 2011, character 16).

38- Anteroposterior development of the postorbital region of the skull: postorbital skull longer than one-third orbital diameter (0), clearly less than one-third orbital diameter (1). (Jiang et al., 2005, character 7).

39- Quadratojugal exposure: extensive (0), small, largely covered by squamosal, postorbital or supratemporal (1). [Campos 2022, character 40 modified from Maisch and Matzke 2000 (character 30) and Fischer et al., 2016 (character 29)].

40- Quadrate neck: clearly demarcated (0), absent, the region anterior to the articular condyle is straight or concave. (Campos 2022, character 41).

41- Occipital lamella of the quadrate: present, giving the lateral surface of the quadrate a U-shape in posterior view (0), reduced, the dorsal part of the quadrate is a simple transversely-compressed lamella (1). (Fischer et al., 2016, character 31).

42- Quadrate angular process: present (0), extremely reduced (1). (Zverkov and Prilepskaya 2019, character 109).

43- Quadrate condyle: massive, strongly expanded (0), weak, mediolaterally compressed (1). (Zverkov and Prilepskaya 2019, character 110).

44- Location of the stapes facet on the posterior surface of the quadrate: on ventral half (0), on dorsal half (1). (Druckenmiller and Maxwell 2010, character 21).

45- Quadrate supratemporal groove: absent (0), present (1). (Zverkov and Efimov 2019, character 37).

46- Basipterygoid processes I: short, giving basisphenoid a square outline in dorsal view (0), markedly expanded laterally, being wing-like, giving basisphenoid a marked pentagonal shape in dorsal view (1). (Fischer et al., 2011, character 18).

47- Basipterygoid processes II: anteriorly directed (0) laterally directed (1). (Modified from Zverkov and Efimov 2019, character 39).

48- Basisphenoid, dorsal view: dorsal plateau appears equal or wider than basioccipital facet, i.e. basioccipital facet oriented mostly posteriorly (0), basioccipital facet appears equal to or wider than dorsal plateau (1). (Maxwell et al., 2016, character 20).

49- Basisphenoid in ventral view: internal carotid foramen (icf) located around the anteroposterior midpoint of the basisphenoid (0); icf located in the posterior third of the basisphenoid (1), icf almost hidden in ventral view and/or located on the basioccipital posterior surface (2). (Campos et al., 2020, character 22, modified from Maxwell et al., 2016, character 22).

50- Extracondylar area of the basioccipital in posterior view: well-developed, with a dorsoventral expansion greater than the height of the occipital condyle (0); developed, but with an expansion smaller than the height of the occipital condyle (1); reduced, but with its lateral and/or ventral portion still visible (2); extremely reduced, not visible in posterior view (3). (Modified from Fernández 2007, character 10).

51- Extracondylar area of basioccipital in lateral view: wide, longer than condylar lateral exposure (0); reduced (1). (Zverkov and Jacobs 2021, character 52).

52- Basioccipital condyle: width and height approximately equal (0), much wider than high (1). (Maxwell et al., 2016, character 24).

53- Basioccipital peg: present (0), absent (1). (Fischer et al., 2011, character 20, modified from Motani 1999, character 29).

54- Ventral notch in the extracondylar area of the basioccipital: present (0), absent (1). (Fischer et al., 2012, character 19).

55- Raised opisthotic facet of the basioccipital: absent (e.g., in lateral view, these facets have a dorsoventral development equivalent to that of the stapedial facets of the basioccipital) (0), present (e.g., in lateral view, these facets have a dorsoventral development smaller than that of the stapedial facets of the basioccipital) (1). (Fischer et al., 2016, character 37).

56- Opisthotic and stapedial facets lateral exposure: well seen (0), poorly seen, shifted anteriorly (1). (Zverkov and Efimov 2019, character 47).

57- Floor of the foramen magnum anteriorly: straight (0), expanded, bilobed (1); constricted (2). (Zverkov and Jacobs 2021, character 58).

58- Location of notochordal pit on the condylar surface of the basioccipital: central (0), dorsal (1). (Moon 2019, character 96).

59- Basis of the exooccipitals: anterior process at the basis of the exooccipital is conspicuously expanded (e.g., in lateral or medial view, the antero-posterior length of the dorsal end of the exoccipital is notably less than the antero-posterior length at the basis) (0), the anterior process at the basis of the exoccipital strongly reduced (e.g., in lateral or medial view, the dorsal end and the basis of the exoccital are approximately equally expanded (1). (Campos et al., 2020, character 67).

60- Prootic, osseous labyrinth shape: impression of the anterior vertical semicircular canal (avsc) to the sacculus (sac)-utriculus (ut) much longer than the width of the ut + sac, i.e., “T”-shaped (0); impression of the avsc to sac-ut distance equal or shorter than width of the ut+sac, i.e., “V”-shaped (1). (Maxwell et al., 2016, character 29).

61- Shape of the paroccipital process of the opisthotic: short and robust (0), elongated and slender (1). (Fischer et al., 2012, character 20).

62- Stapedial facet of the opisthotic: small, mediolaterally narrow (0), or extensive (1). (Zverkov and Jacobs 2021, character 64).

63- Orientation of semicircular canals in the opisthotic: angle between the posterior vertical and horizontal semicircular canals is no less than 90, giving a “T”-shaped outline to the impression (0), less than 90, “V”-shaped (1). (Zverkov and Jacobs 2021, character 65).

64- Ventral part of the impression of the semicircular canals: housing the posterior ampulla and the sacculus not expanded (0); transversely expanded (1). (Zverkov and Jacobs 2021, character 66).

65- Stapedial curvature: absent (0), present (1). (Zverkov and Jacobs 2021, character 67).

66- Stapes proximal head: slender, much smaller than opisthotic proximal head (0), massive, as large or larger than opisthotic (1). (Fischer et al., 2011, character 21, modified from Sander 2000, character 34).

67- Stapedial shaft in adults: thick (0), slender and gracile (1). (Roberts et al., 2014, character 25).

68- Supraoccipital: exoccipital processes parallel (0), exoccipital processes divergent (1). (Maxwell et al., 2016, carácter 19).

69- Lateral margins of the foramen magnum: (0) supraoccipital makes a minor contribution to the foramen magnun (e.g., shallow ventral notch), supraoccipital contribution almost equal to that of exoccipitals (1). (Maxwell et al., 2012, character 20).

70- Dorsal arch of the supraoccipital in posterior view: dorsoventrally thick (e.g., the height of the dorsal arch is equivalent to the width of the exoccipital processes) (0), dorsoventrally thin (e.g., the height of the dorsal arch is smaller than the width of the exoccipital processes) (1). (Modified from Zverkov and Jacobs 2021, character 73).

71- Supraoccipital impression of otic capsule: triradiate with branches of nearly equal length (0), lunate (biradiate) with only two branches well-impressed (1). (Zverkov and Jacobs, character 74).

72- Supraoccipital shape in posterior view: rounded arch (0), squared (1). (Campos 2022, character 73).

73- Articular shape in medial view: trapezoid or quadrate (0), parallelogram-like (1). (Zverkov and Efimov 2019, character 57).

74- Muscular boss on the medial surface of the articular: absent (0), present (1). (Zverkov and Jacobs 2021, character 76).

75- Anterior dentaries: sharply pointed at anterior tip (0), rounded (1). (Maxwell et al., 2016, character 33).

76- Mandibular symphysis I: splenial playing a more extensive role in the mandibular symphysis than the dentary (0), splenial participating in the mandibular symphysis but restricted to the posterior half (1). (Maxwell et al., 2012, character 27, modified from Sander 2000, character 39).

77- Mandibular symphysis II: angulars and splenials subequally exposed immediately anterior to the posteriormost symphysis (0); angulars much less prominent (1). (Maxwell et al., 2016, character 35).

78- Angular lateral exposure: much smaller than surangular exposure (0), extensive (1). (Motani 1999, character 32, inverted coding).

79- Surangular curvature: slight (0), strong (1). (Zverkov and Jacobs 2021, character 81).

80- Musculus adductor mandibulae externus process orientation and development: obliquely vertical, poorly pronounced in dorsal view; nearly horizontal and large, well pronounced in dorsal view (1). (Zverkov and Jacobs 2021, character 82).

81- Morphology of the retroarticular process in lateral view: robust (0), gracile and slender (1). (Campos 2022).

82- Atlas-axis ventral keel: absent (0), present (1). (Zverkov et al., 2015, character 27).

83- Atlas-axis fusion: with pronounced suture (0), no visible suture (1), no fusion (2). (Zverkov and Efimov 2019, character 64).

84- Posterior dorsal/anterior caudal centra: 3.5 times or less as high as long (0), four times or more as high as long (1). (Maxwell 2010, character 15, coding inverted).

85- Tail fin centra: strongly laterally compressed (0), as wide as high (1). (Maxwell 2010, character 16).

86- Neural spines of atlas and axis: completely overlapping, may be fused (0), functionally separate, never fused (1). (Druckenmiller and Maxwell 2010, character 26).

87- Chevrons ossified: present (0), absent (1). (Maisch and Matzke 2000, character 63).

88- Rib – cross-sectional shape at mid-shaft: oval/circular (0); '8' shaped (1); 'T' shaped (2). (Campos 2022, character 89).

89- Coracoid shape in adults: rounded (length to width ratio less than 1.3 and often close to 1) (0), anteroposteriorly elongated (length to width ratio greater or equal to 1.5) (1). (Fischer et al., 2016, character 52, modified from Arkhangelsky and Zverkov 2014, character 53).

90- Anteromedial process of coracoid: poorly pronounced, anteroposteriorly short (0), protruding anteriorly (1), strongly protruding anteriorly along with intercoracoidal facet (2). (Zverkov and Efimov 2019, character 92, modified from Fischer et al. 2016, character 53).

91- Anterior notch of the coracoid: present and prominent (0), extremely reduced or absent (1). (Zverkov and Efimov 2019, character 71, modified from Fischer et al., 2011, character 31).

92- Posterior notch of the coracoid: present (0); absent (1). (Moon 2019, character 186, modified from Maxwell et al., 2012, character 34).

93- Coracoid medial facet: relatively thin (0), extremely thickened dorsoventrally (1). (Zverkov and Efimov 2019, character 72).

94- Demarcation of scapular and glenoid facets of the coracoid in adults: clearly demarcated (0), poorly demarcated (1). (Zverkov and Jacobs 2021, character 96).

95- Relative size of scapular facet and glenoid contribution of the coracoid: scapular facet much smaller than the glenoid (50% or less) (0), comparable in size (70% or more). (Zverkov and Jacobs 2021, character 97).

96- Glenoid contribution of the scapula: extensive, being at least as large as the coracoid facet (0), reduced, being markedly smaller than the coracoid facet. (Fischer et al., 2012, character 27).

97- Prominent acromion process of scapula: absent (0), present (1), very large and set off ventrally (2). (Zverkov and Jacobs 2021, character 99, modified from Fischer et al. 2011, character 31).

98- Scapular coracoid facet and acromion process: continuous (0), separated by a notch of complete ossification (1). (Zverkov and Jacobs 2021, character 100).

99- Scapular shaft: strap-like (0), rod-like (1). (Zverkov and Efimov 2019, character 75).

100- Interclavicle p.m.s. shape: strap-like or rod-like but relatively slender (0), markedly expanded (1). (Zverkov and Efimov 2019, charcter 76).

101- Interclavicle: median stem is equal to or longer than the transverse bar (0), Transverse bar is longer than median stem (1). (Delsett et al., 2019, character 102).

102- Interclavicle ventral knob: absent (0), present (1). (Zverkov and Efimov 2019, character 77).

103- Plate-like dorsal ridge on humerus: absent (0), present (1). (Motani 1999, character 56).

104- Protruding triangular deltopectoral crest on humerus: absent (0); present (1). (Fischer et al., 2011, character 31).

105- Relative length of the humerus in the midshaft in dorsal/ventral view: midshaft with a pronounced constriction (0), midshaft of a length similar to that of the epiphyses (1). (Campos 2022, character 105).

106- Humerus distal and proximal ends in dorsal view: distal end wider than proximal end (0), nearly equal or proximal end slightly wider than distal end (1). (Fischer et al., 2011, character 32, modified from Motani, 1999, character 55).

107- Anterodistal facet of the humerus for an anterior accessory element to the radius: absent (0), present but poorly developed (1), present and very well developed, forming a triangular/square surface (2). (Campos 2022, character 107).

108- Humerus with posterodistally deflected ulnar facet and distally facing radial facet: absent (0), present (1). (Fischer et al., 2012, character 34, modified from Fischer et al. 2011, character 34).

109- Posterior third of the humeral shaft: not compressed, posterior edge of the shaft strongly concave (0), compressed, and posterior edge of the gently concave (1). (Campos et al., 2020, character 68).

110- Humerus/intermedium contact: absent (0); present (1). (Fernández 2007, character 16).

111- Shape of the posterior surface of the ulna: rounded or straight and nearly as thick as the rest of the lament (0), concave and edgy (1). (Fischer et al., 2012, character 36).

112- Posterior accessory epipodial element posterior to ulna: absent (0), present (1), present with associated facet on humerus (2). (Fischer et al., 2016, character 64).

113- Manual pisiform: absent (0); present (1); present and reaching humerus (2). (Zverkov and Jacobs 2021, character 117, modified from Fischer et al., 2011, character 36).

114- Notching of anterior facet of leading edge elements of forefin in adults: present (0), absent (1). (Fischer et al., 2011, character 37, modified from Motani 1999, characters 59 and 65).

115- Intermedium: distal edge angular (0), distal edge flattened (1). (Maxwell 2010, character 27).

116- Shape of aae: aae absent (0), lunate (1), rounded/squared (2). (modified from Zverkov and Efimov 2019, character 85).

117- Posterior enlargement of forefin (number of postaxial accessory 'complete' digits): none (0); one (1), two or more (2). (Fischer et al., 2011, character 38, modified from Maisch and Matzke 2000, character 89).

118- Preaxial accessory digits on forefin: absent (0), one (1), two or more (2). (Fischer et al., 2016, character 69, modified from Maisch and Matzke 2000, character 91).

119- Number of digits directly supported by the intermedium: one (0), two (1). (Fischer et al., 2011, character 40).

120- Zeugo- to autopodial elements: flattened and plate-like (0), strongly thickened (1). (Maisch and Matzke 2000, character 94).

121- Tightly packed rectangular phalanges: absent, phalanges are mostly rounded (0), present (1). (Fischer et al., 2011, character 42, modified from Maisch and Matzke 2000, character 102).

122- Ischium-pubis fusion in adults: absent or present only proximally (0), present with an obturator foramen (1), present with no obturator foramen (2). (Fischer et al., 2011, character 44, modified from Mazin 1982, character 13).

123- Ischium or ischiopubis shape: plate-like, flattened (0), rod-like (1). (Fischer et al., 2011, character 45, modified from Motani 1999, character 87).

124- Prominent, ridge-like dorsal and ventral processes demarked from the head of the femur and extending up to mid-shaft: absent (0), present (1). (Fischer et al., 2011, character 46).

125- Ventral process on femur: smaller than dorsal process (0), more prominent (1). (Roberts et al., 2014, character 52).

126- Astragalus/femoral contact: absent (0), present (1). (Maxwell 2010, character 33).

127- Femur anterodistal facet for accessory zeugopodial element anterior to tibia: absent (0); present (1). (Fischer et al., 2011, character 48).

128- Distal end of the femur in dorsal/ventral view: more developed and expanded than the proximal end (0); less developed than the proximal end (1). (modified from Fischer et al., 2013, character 61).

129- Hindfin leading edge element in adults: notched (0); straight (1). (Fischer et al., 2013, character 65, modified from Motani 1999, character 92).

130- Postaxial accessory digits in the hindfin: absent (0); present (1). (Fischer et al., 2011, character 50).

SUPPLEMENTARY REFERENCES

Arkhangelsky, M.S. and Zverkov, N.G. 2014. On a new ichthyosaur of the genus Undorosaurus. Proceedings of the Zoological Institute RAS 318:187-196.

Bardet, N. and Fernández, M.S. 2000. A new ichthyosaur from the Upper Jurassic lithographic limestones of Bavaria. Journal of Paleontology 74:503-511.

Bauer, F. 1898. Die Ichthyosaurier des oberen weissen Jura. Palaeontographica 44:283-328.

Campos, L. 2022. Oftalmosáuridos (Ichthyosauriomorpha: Ichthyosauria) del Jurásico Tardío-Cretácico Temprano de Patagonia Argentina: diversidad, disparidad y evolución. (Unpubl. PhD thesis). Universidad Nacional de La Plata, Buenos Aires.

Campos, L., Fernández, M.S., and Herrera, Y. 2020. A new ichthyosaur from the Late Jurassic of north-west Patagonia (Argentina) and its significance for the evolution of the narial complex of the ophthalmosaurids. Zoological Journal of the Linnean Society 188:180-201.

Campos, L., Fernández, M.S., Herrera, Y., and Talevi, M. 2025. Eternauta patagonica gen. et sp. nov.: a new ophthalmosaurid ichthyosaur from the Upper Jurassic of Patagonia and its palaeoecological implications. Historical Biology In Press. https://doi.org/10.1080/08912963.2025.2568707

Delsett, L.L., Roberts, A.J., Druckenmiller, P.S., and Hurum, J.H. 2019. Osteology and phylogeny of Late Jurassic ichthyosaurs from the Slottsmoya Member Lagerstätte (Spitsbergen, Svalbard). Acta Palaeontologica Polonica 64:717-743.

Druckenmiller, P.S. and Maxwell, E.E. 2010. A new lower Cretaceous (lower Albian) ichthyosaur genus from the Clearwater Formation, Alberta, Canada. Canadian Journal of Earth Sciences 47:1037-1053.

Fernández, M.S. 2007. Redescription and phylogenetic position of Caypullisaurus (Ichthyosauria: Ophthalmosauridae). Journal of Paleontology 81:368-375.

Fernández, M.S., Archuby, F., Talevi, M., and Ebner, R. 2005. Ichthyosaurian eyes: paleobiological information content in the sclerotic ring of Caypullisaurus (Ichthyosauria, Ophthalmosauria). Journal of Vertebrate Paleontology 25:330-337.

Fischer, V., Appleby, R.M., Naish, D., Liston, J., Riding, J.B., Brindley, S., and Godefroit, P. 2013. A basal thunnosaurian from Iraq reveals disparate phylogenetic origins for Cretaceous ichthyosaurs. Biology Letters 9:20130021.

Fischer, V., Bardet, N., Benson, R.B., Arkhangelsky, M.S., and Friedman, M. 2016. Extinction of fish-shaped marine reptiles associated with reduced evolutionary rates and global environmental volatility. Nature communications 7:10825.

Fischer, V., Maisch, M.W., Naish, D., Kosma, R., Liston, J.J., Joger, U., Kruger, F.J., Pérez, J.P., Tainsh, J., and Appleby, R.M. 2012. New ophthalmosaurid ichthyosaurs from the European Lower Cretaceous demonstrate extensive ichthyosaur survival across the Jurassic-Cretaceous boundary. PLoS ONE 7:e29234.

Fischer, V., Masure, E., Arkhangelsky, M.S., and Godefroit, P. 2011. A new Barremian (Early Cretaceous) ichthyosaur from western Russia. Journal of Vertebrate Paleontology 31:1010-1025.

Jiang, D.Y., Hao, W. C., Maisch, M.W., Matzke, A.T., and Sun, Y.L. 2005. A basal mixosaurid ichthyosaur from the Middle Triassic of China. Palaeontology 48:869-882.

Maisch, M.W. and Matzke, A.T. 2000. The Ichthyosauria. Stuttgarter Beiträge zur Naturkunde: Serie B (Geologie und Paläontologie) 298:1-59.

Massare, J.A. and Connely, M.V. 2022. Braincase morphology of Baptanodon natans (Reptilia: Ichthyosauria). Paludicola 14:43-56.

Maxwell, E.E. 2010. Generic reassignment of an ichthyosaur from the Queen Elizabeth Islands, northwest territories, Canada. Journal of Vertebrate Paleontology 30:403-415.

Maxwell, E.E., Fernandez, M.S., and Schoch, R.R. 2012. First diagnostic marine reptile remains from the Aalenian (Middle Jurassic): a new ichthyosaur from southwestern Germany. PLoS ONE:e41692.

Maxwell, E.E., Dick, D., Padilla, S., and Parra, M.L. 2016. A new ophthalmosaurid ichthyosaur from the Early Cretaceous of Colombia. Papers in Palaeontology 2:59-70.

Meyer, H. 1863. Ichthyosaurus leptospondylus Wag.? aus dem lithographischen Schiefer von Eichstätt. Palaeontographica 11:222-225.

Moon, B.C. 2019. A new phylogeny of ichthyosaurs (Reptilia: Diapsida). Journal of Systematic Palaeontology 17:129-155.

Motani, R. 1999. Phylogeny of the Ichthyopterygia. Journal of Vertebrate Paleontology 19:473-496.

Roberts, A.J., Druckenmiller, P.S., Sætre, G.P., and Hurum, J.H. 2014. A new Upper Jurassic ophthalmosaurid ichthyosaur from the Slottsmøya Member, Agardhfjellet Formation of central Spitsbergen. PLoS ONE 9:e103152.

Sander, P.M. 2000. Ichthyosauria: their diversity, distribution, and phylogeny. Paläontologische Zeitschrift 74:1-35.

Serafini, G., Maxwell, E.E., Fornaciari, E., and Papazzoni, C.A. 2022. Revision of platypterygiine rostral material from the Northern Apennines (Italy): new insights on distal neurovascular anatomy and tooth replacement in Cretaceous ichthyosaurs. Cretaceous Research 135:105167.

Zverkov, N.G. and Efimov, V.M. 2019. Revision of Undorosaurus, a mysterious Late Jurassic ichthyosaur of the Boreal Realm. Journal of Systematic Palaeontology 17:1183-1213.

Zverkov, N.G. and Jacobs, M.L. 2021. Revision of Nannopterygius (Ichthyosauria: Ophthalmosauridae): reappraisal of the ‘inaccessible’ holotype resolves a taxonomic tangle and reveals an obscure ophthalmosaurid lineage with a wide distribution. Zoological Journal of the Linnean Society 191:228-275.

Zverkov, N.G. and Prilepskaya, N.E. 2019. A prevalence of Arthropterygius (Ichthyosauria: Ophthalmosauridae) in the Late Jurassic--earliest Cretaceous of the Boreal Realm. PeerJ 7:e6799.

Zverkov, N.G., Arkhangelsky, M.S., and Stenshin, I.M. 2015. A review of Russian Upper Jurassic ichthyosaurs with an intermedium/humeral contact. Reassessing Grendelius McGowan, 1976. Proceedings of the Zoological Institute RAS 319:558-588.

APPENDIX 3.

Character-taxon matrix (.nex). This file available for download at https://palaeo-electronica.org/content/2026/5919-late-jurassic-ichthyosaurs-from-germany